



**Politecnico
di Torino**

Department of Mechanical and Aerospace Engineering

Master's Degree Program in Aerospace Engineering

Master Thesis

Conceptual design methodology for
estimating chemical emissions and
analysing pollutant dispersion in
suborbital flight carriers

Candidate

Gnaccarini Sara (330309)

Supervisor

Fusaro Roberta

Co-Supervisor

Viola Nicole

Borgna Fabrizio

Academic Year: 2024-2025

Contents

| | | |
|----------|--|-----------|
| 1 | Introduction | 4 |
| 2 | Suborbital Flight: an overview | 5 |
| 3 | Case study: White Knight Two carrier | 10 |
| 3.1 | Reference mission description | 12 |
| 4 | State of the art | 16 |
| 4.1 | Chemical emission assessment methods | 16 |
| 4.1.1 | ICAO LTO cycle emissions formulation | 16 |
| 4.1.2 | P3-T3 method | 17 |
| 4.1.3 | Boeing Fuel Flow Method 2 | 19 |
| 4.2 | Local air quality impact assessment methods | 24 |
| 4.2.1 | Analytical dispersion models | 25 |
| 4.2.2 | Software and Tools | 33 |
| 5 | Methodology | 42 |
| 5.1 | Chemical emissions assessment - LTO cycle | 42 |
| 5.2 | Chemical emissions assessment - reference mission | 43 |
| 5.2.1 | Humidity correction factor | 44 |
| 5.2.2 | ASTOS data collection | 45 |
| 5.2.3 | Takeoff and Landing ground-roll implementation method- ology | 46 |
| 5.3 | Air quality impact assessment | 50 |
| 5.3.1 | Evaluation of NO_x average concentration in the engine plume | 50 |
| 5.3.2 | WK2 LTO Cycle Dispersion Analysis Using LASPORT . | 51 |
| 6 | Chemical emissions estimation results | 54 |
| 6.1 | White Knight Two LTO cycle emissions | 54 |
| 6.1.1 | A comparison: LTO cycle emissions by Boeing 747 LCF Dreamlifter | 57 |
| 6.2 | White Knight Two reference mission emissions | 59 |
| 7 | Air quality impact assessment results | 67 |
| 7.1 | NO_x average concentration in the engine plume - analytical model | 67 |
| 7.2 | Assessment of NO_x dispersion during WK2 LTO cycle opera- tions using LASPORT | 69 |

| | | |
|----------|------------------------------------|-----------|
| 7.2.1 | Calculation setup | 69 |
| 7.2.2 | Calculation results | 70 |
| 8 | Conclusion and future works | 75 |

Abstract

Suborbital flights are highly versatile and offer several opportunities to make rapid progress in various scientific fields and to develop new business activities. Concurrently, the growing concern over the environmental impact of the aviation sector highlights the need to assess and analyse the chemical emissions and their impacts on both climate change and local air quality.

This thesis aims to bridge these two aspects, exploring the potential of suborbital flights while also evaluating their environmental implications. It focuses on the carrier of an A-to-A suborbital flight, namely White Knight Two, with Grottaglie as the reference spaceport. The first part concentrates on the assessment of the chemical emission of both proportional and non-proportional species during the ICAO Landing and Takeoff (LTO) cycle and along the nominal trajectory, described by AS-TOS simulation, applying the Boeing Fuel Flow Method 2. These data are then compared and validated against a certified dataset reported in the literature.

The research proceeds with an investigation on methods for assessing local air quality. It begins with an in-depth literature review of analytical dispersion models, as well as commercial software and tools. This is followed by the implementation of a simplified Gaussian Plume model to evaluate NO_x concentrations during the landing and takeoff cycle, which is then validated using experimental data from existing studies. A comparison is then made between the resulting NO_x concentrations produced by the WK2 carrier and those of the Boeing 747 LCF Dreamlifter, which operates regular flights at the reference airport. The aim is to show the public that WK2 and SS2 flights are not more impactful on air quality than the commercial flights already in operation.

The final part is intended to serve as a starting point for future studies that may focus on assessing local air quality around the airport. These studies could take into account typical daily traffic at the spaceport, along with all the nearby emission sources, in order to accurately evaluate the long-term impact of aviation activities on the surrounding population.

1 Introduction

The aim of this thesis is to bring together two emerging aspects of the aerospace field: the exploration and development of suborbital flight, and the growing concerns about the environmental impact of this sector.

Suborbital flights are considered a promising concept for new forms of travel, astronaut training, scientific experimentation, and even leisure activities involving microgravity. However, it is important to keep in mind the need to minimize the environmental impact of such operations in order to make them sustainable, even at high frequencies.

This work aims to evaluate the potential environmental impact of a carrier aircraft used in suborbital flight operations. Specifically, the White Knight Two carrier of Virgin Galactic’s air-launched suborbital system has been selected as a case study. The reference mission considered is an A-to-A suborbital flight from and to Grottaglie spaceport, which is currently under evaluation by ENAC (Ente Nazionale per l’Aviazione Civile).

After a brief introduction on suborbital flight and the White Knight Two vehicle and SpaceShipTwo characteristics and mission, an extensive chapter is dedicated to describing the state of the art relative to chemical emissions estimation methods and local air quality assessment methods, and tools.

The methodology used to conduct the analysis is presented in a dedicated chapter. It involves the Boeing Fuel Flow Method 2 for estimating chemical emissions along the reference trajectory, an analytical Gaussian plume model for calculating pollutant concentrations, and a simulation setup for dispersion analysis during LTO cycle operations up to 895 m, carried out using the LAS-PORT software.

The results of this study include the total amount of emitted chemical species (both proportional and non-proportional) along the mission profile, the average concentration of NO_x in the engine plume during the takeoff phase (assuming a continuous and steady emission source), and the NO_x dispersion analysis during the departure (takeoff and climb up to 895 m), arrival (approach and landing), and idle phases.

The presented outcomes can serve as a starting point for more detailed future analyses and support the feasibility of operating horizontal take-off and landing suborbital flights from Grottaglie Airport without significantly affecting local air quality.

2 Suborbital Flight: an overview

The space industry is constantly evolving, and the new market of commercial space transport has recently emerged. This sector has the potential to revolutionize how space will be accessed in the future, and one of its most promising aspects is suborbital flight.

Suborbital flights are highly versatile and offer several opportunities to make rapid progress in various scientific fields and to develop new business activities. For example, they can be used for microgravity experiments, astronauts' training, testing payloads and instruments for future space missions, cargo transport, as well as for commercial and tourism purposes.

The growing interest in suborbital flights, along with the involvement of private companies in the space sector, has highlighted the need to develop a dedicated regulatory framework that can work alongside existing civil aviation and airspace systems. Until recently, space operations were mostly carried out by research centers or space agencies within segregated areas. However, this approach is no longer sustainable, as air traffic is expected to increase in the coming years. A well-structured regulatory framework will help ensure an adequate level of safety for third parties on the ground, in the air, and at sea, as well as for people on board.

In accordance with ICAO (International Civil Aviation Organization) a suborbital flight is a flight beyond 100 kilometers above sea level in which the vehicle does not attain the speed to escape Earth's gravity field. They can be further categorized depending on their path:

- Local (A-to-A) suborbital flight = a suborbital operation carried out by a vehicle not intended to land at a destination different than (or far from) departure (launch/take-off site coincides with the return/landing site) [10];
- Long distance (A-to-B) suborbital flight = a suborbital operation carried out by a vehicle intended to land at a destination different than departure [10].

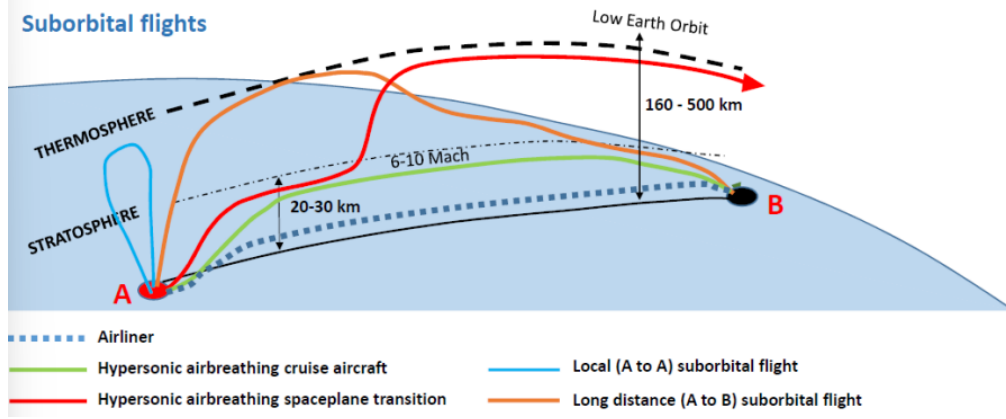


Figure 1: Illustration of Suborbital Flights [31]

Suborbital flights can be carried out using different types of suborbital vehicles, depending on the design's philosophy. A possible classification may be the following:

- Vertical Take-off and Horizontal Landing;
- Horizontal Take-off and Landing;
- Air-Launched;

Hereafter are reported brief descriptions and examples for each category identified.

An example of the first class identified is the *SpaceLiner*: a hypersonic, winged passenger transporter, which could also serve as a low-cost solution for launching satellites into orbit in a variant equipped with a payload bay [14].

The system consists of two stages: an uncrewed booster and a passenger stage (called the orbiter stage), and it is intended to have a vertical launch. It is designed to carry 50 passengers and is powered by a total of 11 LOX-LH2 liquid rocket engines (9 in the booster stage and 2 in the orbiter stage).

After main engine cut-off, the passenger stage glides across large intercontinental distances in a short time. Depending on the mission profile, it is possible to reach flight altitudes of up to 80 km and Mach numbers well above 20.

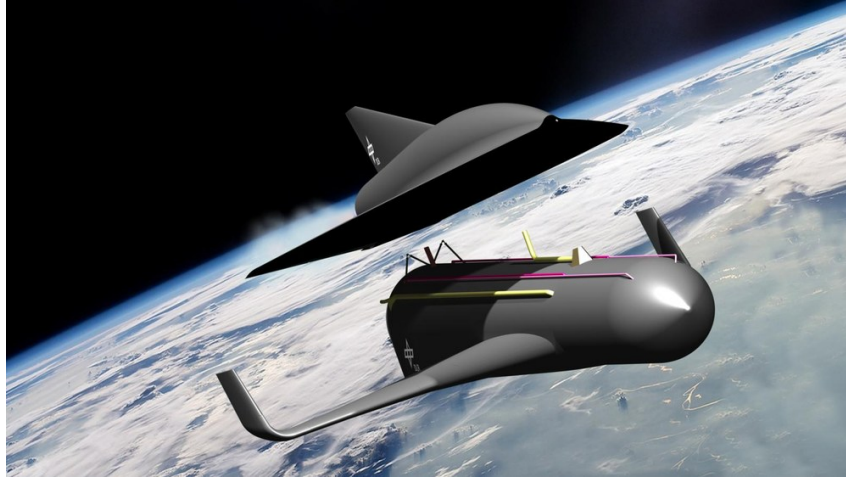


Figure 2: SpaceLiner - detachment of the booster stage from the orbiter one

Regarding the category of horizontal takeoff and landing spaceplanes, an example could be the XCOR Lynx Mark II: it is a two-seat commercial reusable launch vehicle developed by the California-based company XCOR Aerospace. It is powered by four LOX-kerosene liquid rocket engines and it can carry a pilot, a ticketed passenger, payload or small satellites for a suborbital flight.



Figure 3: XCOR Lynx Mark II

Another example of this group is the Skylon: it is a single stage to orbit (SSTO) vehicle developed by Reaction Engine LDt in the UK. It can takeoff and land on a runway delivering 15mT of payload into LEO orbit. It is unmanned and it is powered by two innovative dual-mode SABRE engines. This

engine is based on a rocket engine that uses liquid hydrogen for fuel and ignites with either liquid oxygen or air, depending on the operational mode. In detail:

- Airbreathing mode (active under 28.5 km altitude and Mach 5): an innovative helium loop system chills and compresses the ingested air to an almost liquid state to be used by the rocket engine;
- Rocket mode (active above 28.5 km altitude and Mach 5): liquid oxygen is supplied from the tanks to complete the ascent.

Combining these capabilities into one system permits to reduce the mass of launching and to eliminate the need to have multiple stages.



Figure 4: Skylon

For the last category, the Virgin Galactic system, consisting of White Knight Two (the carrier aircraft) and SpaceShipTwo (the spacecraft), can be taken as an example.

Takeoff and initial climb are performed solely using the thrust from WK2's four turbofan engines while the two vehicles are in the mated configuration. Once the release altitude is reached, SS2 is undocked from WK2 and begins its ascent, powered by a hybrid rocket engine. This is followed by a coasting phase to reach the target altitude of 100 km. Reentry occurs in a special "feathered" configuration, which maximizes drag without damaging the spacecraft. The final approach and landing are then performed in the standard (unfeathered) configuration.



Figure 5: White Knight Two and SpaceShipTwo in mated configuration

This thesis will focus on White Knight Two carrier from Virgin Galactic, as representative for air-launched suborbital flight, and in particular, it will consider an A-to-A suborbital flight, with Grottaglie as the reference spaceport.

3 Case study: White Knight Two carrier

This thesis will focus on White Knight Two mission, which consists of transporting SpaceShipTwo up to the release altitude, enabling it to start its ascent, and then coming back to the departure airport.

The suborbital launch architecture consists of two vehicles: SpaceShipTwo (SS2) and its carrier aircraft, White Knight Two (WK2).

SpaceShipTwo (SS2) is a hybrid-rocket-powered, reconfigurable prototype developed by Scaled Composites for Virgin Galactic's commercial spaceflight program. Designed to carry two pilots and at least six passengers on a vertical suborbital flight, the vehicle aims to reach an apogee of roughly 110 kilometres. SS2 is first carried to high altitude beneath its dedicated mothership, WhiteKnightTwo (WK2). Once released, it ignites its rocket motor to start climbing to its suborbital peak. A coasting phase then follows, taking it to apogee. Afterward, it re-enters the atmosphere using a unique "feathered" configuration that maximizes aerodynamic drag without damaging the spacecraft. Finally, it transitions to an unfeathered state, glides, and lands on a conventional runway at the departure airport.

Every flight starts with SS2 mounted beneath WK2. After take-off, WK2 climbs to roughly 15000 m, where it releases the spacecraft. SS2 then lights its hybrid rocket motor, accelerates to about Mach 1, and passes through a brief "pitch bobble" (a nose-up, then nose-down oscillation) as it transitions to supersonic speed.

For Virgin Galactic's nominal profile, the motor shuts down near 45000 m. SS2 then coasts ballistically to its apogee, deploys the feather, and begins its descent. In the feathered configuration the tail swings up, placing the vehicle in a high-drag, attitude-stable posture that limits g-loads and aero-heating during re-entry. After slowing back below Mach 1, the tail is stowed, transforming SS2 into a glider for a standard runway landing.

The spaceship is provided with some feather locks, which are crucial while the tail is down: during the transonic "bobble" the tail can experience large upward aerodynamic loads that might overpower the actuators. The locks prevent any uncommanded feather deployment until the vehicle is safely past this regime [33].



Figure 6: White Knight Two and Space Ship Two in mated configuration [5]

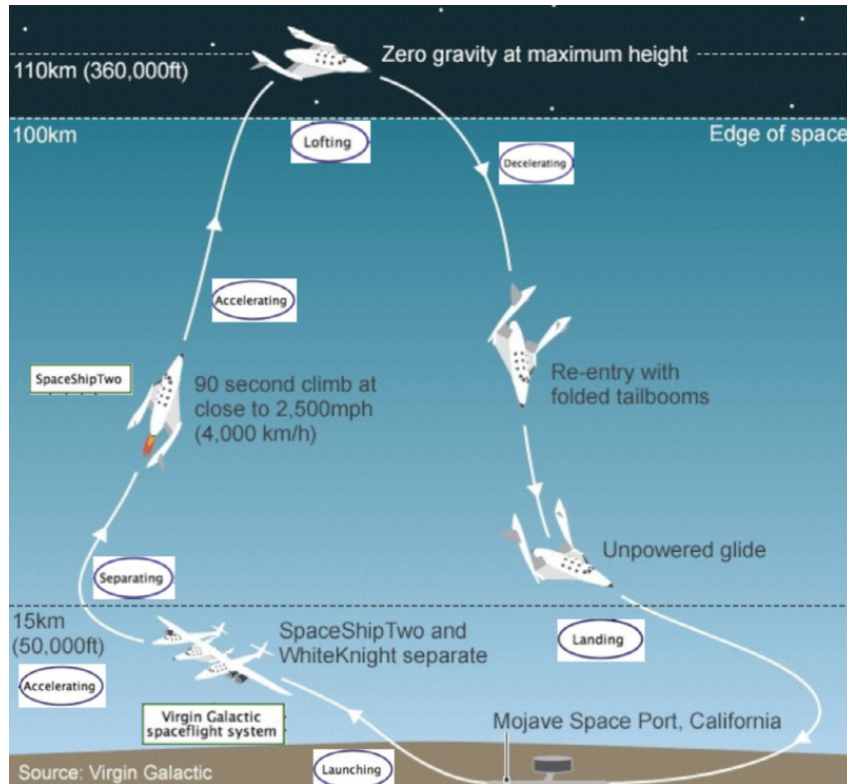


Figure 7: White Knight Two and Space Ship Two mission

WK2 is the largest all-carbon-composite construction aircraft in service [45]; it features structural strength, exceptional climb performance, and heavy lift to high altitude capability that allows unprecedented operational flexibility for a multitude of applications.

It is a twin-fuselage aircraft, featuring a unique 'catamaran' design with an unswept, single-piece wing. This catamaran airframe configuration allows for flexible payload placement and configuration. Indeed, the fuselages are posi-

tioned 13.7 m apart by WK2 inverted gull wing, in order to offer unobstructed ground access and an open architecture approach that maximizes utility and flexibility for different missions.

The aircraft is powered by four Pratt & Whitney Canada PW308A turbofan engines with a total installed thrust of 123 kN, which are controlled for fuel efficiency reasons by the FADEC. This is a certified engine, so it figures on the ICAO Emission Databank [12], which provides all the necessary information to proceed with the chemical emission estimation.

The main characteristics of WK2 are reported in Table 1.

| Height | Wing Span | Lenght |
|------------------|-------------------------------|--------------------|
| 7.9 m | 42.7 m | 23.7 m |
| Service Ceiling | MTOW | Range (no payload) |
| >16700 m | 31840 kg | 4815 km |
| BFL at ISO, MTOW | Max Payload mass | Max fuel load |
| <2440 m | 13600 kg | 9700 kg |
| Max Cruise Speed | Takeoff distance (no payload) | Installed Thrust |
| Mach = 0.65 | 823 m | 123 kN |

Table 1: WK2 charatcteristics [45]

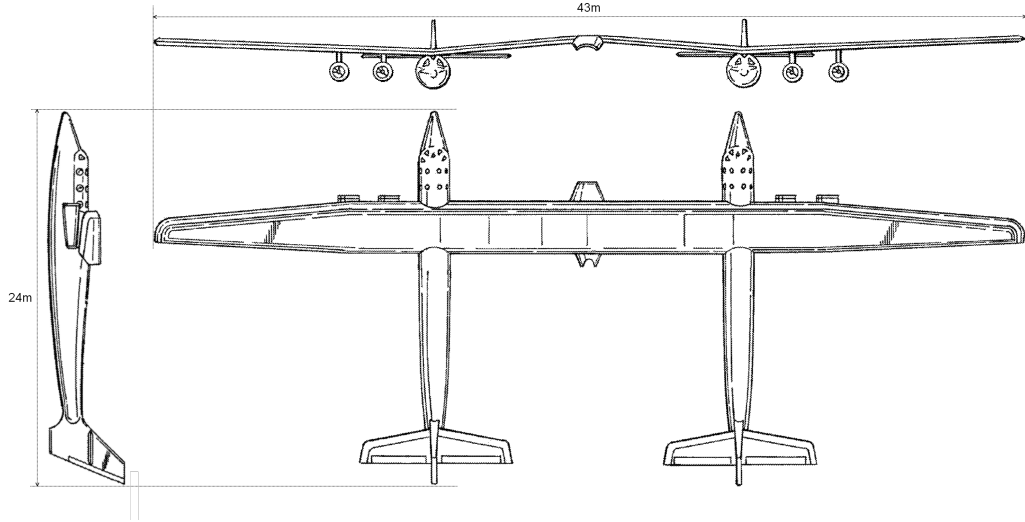


Figure 8: Three-view WK2 drawing

3.1 Reference mission description

The case-study for the thesis is the A-to-A suborbital flight from Taranto-Grottaglie airport.

In May 2018, it was announced that the Taranto-Grottaglie Airport had been

selected by the Ministry of Infrastructure and Transport for the construction of Italy's first operational spaceport for suborbital flights. The selection of the site for the Italian spaceport follows the agreement signed in December 2017 between Turin-based ALTEC (a company owned by ASI and Thales Alenia Space), Sitael (a company of the Angel Group), and Richard Branson's Virgin Galactic. According to the agreement between those companies, the operational possibilities of the Italian spaceport are being jointly evaluated for Virgin Galactic to carry out experimental suborbital flights, astronaut and pilot training, educational purposes and space tourism also following the 2014 'Memorandum of cooperation in the development of commercial space transportation' agreement signed between ENAC (Ente Nazionale per l'Aviazione Civile) and FAA (Federal Aviation Administration), and renewed in 2016, and the cooperation agreement between the American FAA, ENAC and ASI (Agenzia Spaziale Italiana) on "Commercial Space Transportation" signed in June 2017 at the "Casa dell'Aviatore" of the Aeronautica Militare. In October 2020, ENAC's board of directors approved the regulations for the construction and operation of the airport, providing an official endorsement for the adaptation of the facility. In addition, in November 2023, ENAC published the first edition of the "Suborbital and access to space operations (SASO) regulation", and, in December 2023, the third edition of the "Regolamento per la costruzione e l'esercizio degli spaziporti".

The reference mission of White Knight Two carrier can be described by the following phases:

| Phase | Configuration | Description | Duration [min] |
|----------|---------------|--|----------------|
| Taxi out | WK2+SS2 | On-ground movement from gate to runway | 13 |
| Takeoff | WK2+SS2 | Acceleration to takeoff speed | 1 |
| Climb | WK2+SS2 | Climb to the release altitude with spiral trajectory | 40 |
| Cruise | WK2+SS2 | Cruise phase needed to reach optimal condition for release | 5 |
| Release | WK2+SS2 | SS2 disengages from WK2 | 3 s |
| Descent | WK2 | Subsonic descent | 40 |
| Landing | WK2 | Touchdown and deceleration to a complete stop | 1 |
| Taxi in | WK2 | On-ground movement from runway to gate | 13 |

Table 2: White Knight Two reference mission phases

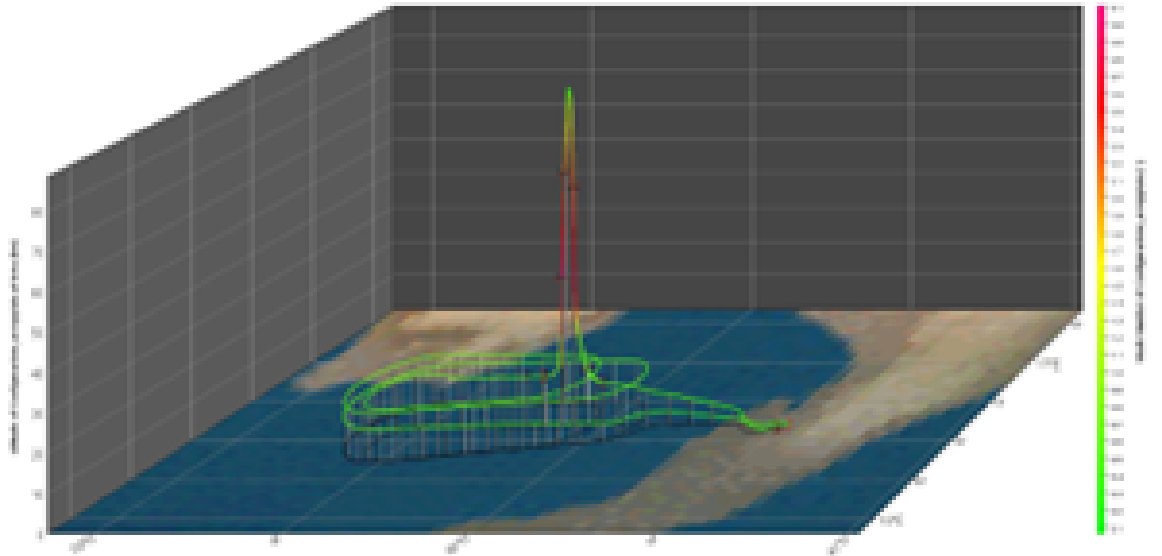


Figure 9: Complete mission profile WK2 and SS2

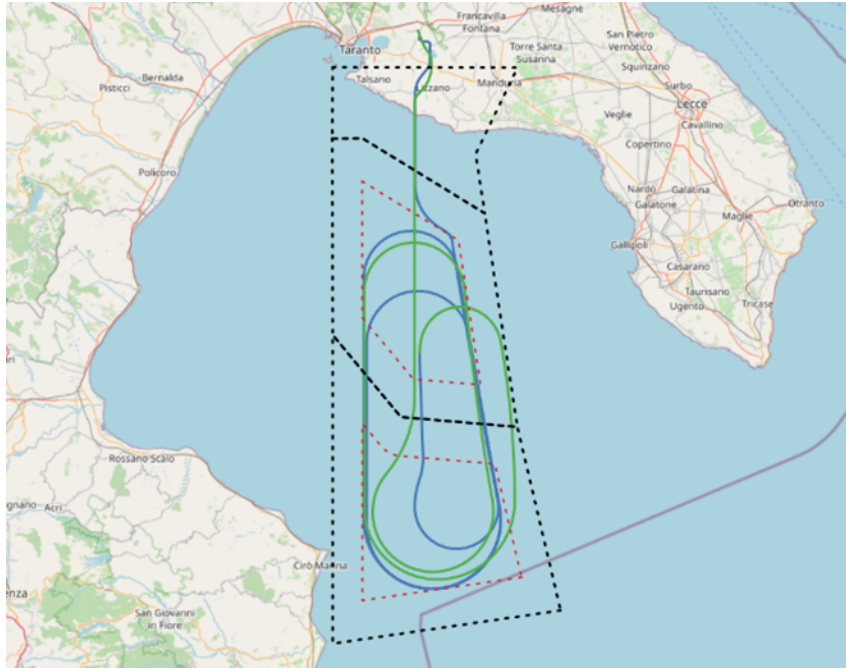


Figure 10: WK2 mission profile

4 State of the art

This section provides an overview of the current state of the art in chemical emissions estimation methods and local air quality impact assessment techniques.

4.1 Chemical emission assessment methods

Since the late 1970s, the International Civil Aviation Organization (ICAO) has been developing measures to address emissions from aircraft engines to limit the sector’s environmental impact. To produce the required thrust, a combustion of kerosene with air happens, and various chemically and radiatively active species are released from the aircraft into its wake. These emissions interact with the surrounding atmosphere, altering its natural chemical balance and contributing to air quality concerns and human-induced climate change. The amount of a given emission produced per unit mass of fuel burnt is commonly known as the emission index (EI) and is expressed in grams of emission per kilogram of fuel consumed [g/kg].

Depending on the species being analyzed, the emission index may remain constant or vary throughout the mission. For instance, the indices for CO_2 , H_2O , and SO_x remain consistent across the entire flight cycle, while CO , HC , NO_x , and soot emissions are significantly influenced by a wide range of variables, particularly engine power settings and environmental conditions at the engine inlet. The first two are higher at low power settings because they are products of incomplete combustion, while the latter two are products of the high temperatures reached in the combustion chamber, making them appear at high power settings.

4.1.1 ICAO LTO cycle emissions formulation

Aircraft engine emissions can significantly affect air quality, especially in the proximity of airports and must be taken into account in the engine certification process, which is based on LTO (landing and take-off) cycle emissions. This standard near-ground operations cycle, defined by the ICAO for certification purposes, comprises four modes defined by the level of thrust and phase duration:

- Take-off: 100% available thrust for 0.7 minutes;

- Climb: 85% available thrust for 2.2 minutes;
- Approach: 30% available thrust for 4 minutes;
- Idle: 7% available thrust for 26 minutes.

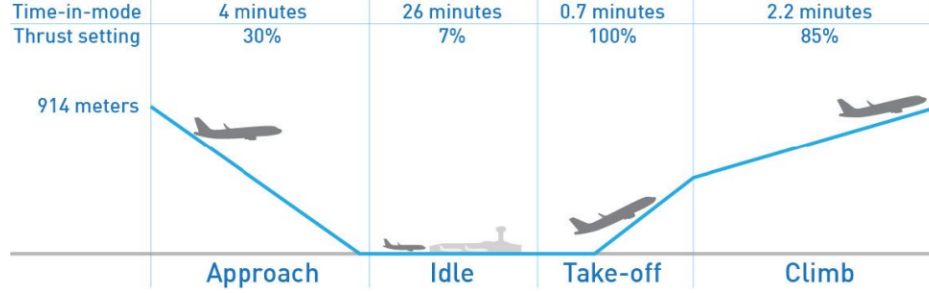


Figure 11: ICAO LTO cycle

The data required to calculate LTO cycle emissions is in the ICAO Engine Emissions Databank [2]. This database contains data on exhaust emissions from certified aircraft engines (emission indices of non-proportional species as long as fuel flow rate for each LTO cycle phase), specifically turbojet and turbofan engines with a static thrust greater than 26.7 kN, measured according to the procedures outlined in ICAO Annex 16, Volume II, and, where applicable, certified by the States of Design of the engines in accordance with their national regulations. The data is provided by the engine manufacturers.

4.1.2 P3-T3 method

The $P_3 - T_3$ method allows for the calculation of NOx, HC, and CO emissions over a reference trajectory. It is the preferred method for calculating aircraft engine emissions, but it requires knowledge of the total pressure P_3 and total temperature T_3 at the high compressor exit/ combustor diffuser inlet, as well as engine fuel flow and ambient atmospheric humidity.

The method is based on the application of semi-empirical correlations of emissions with P_3 and T_3 .

The fundamental steps to conduct the emission analysis using $P_3 - T_3$ method are listed below [9]:

1. Definition of the aircraft mission;

2. Running the aircraft performance prediction code to obtain in output thrust, fuel flow, time, pressure, altitude, flight speed, and ambient temperature, for every discrete point of the mission;
3. Running the engine performance model using as input the data collected at the previous step to obtain as output T_3 values for each mission point;
4. Calculation of the emission indices of NOx, HC, and CO at sea level, a reference sea level compressor exit pressure P_{3SL} , and FAR (fuel-to-air ratio) for each point of the mission using T_{3Alt} coming from the previous step as input;
5. Calculation of the emission indices at the proper altitude for each mission point using the correction formulation expressed below;
6. Calculation of the total emission during the mission.

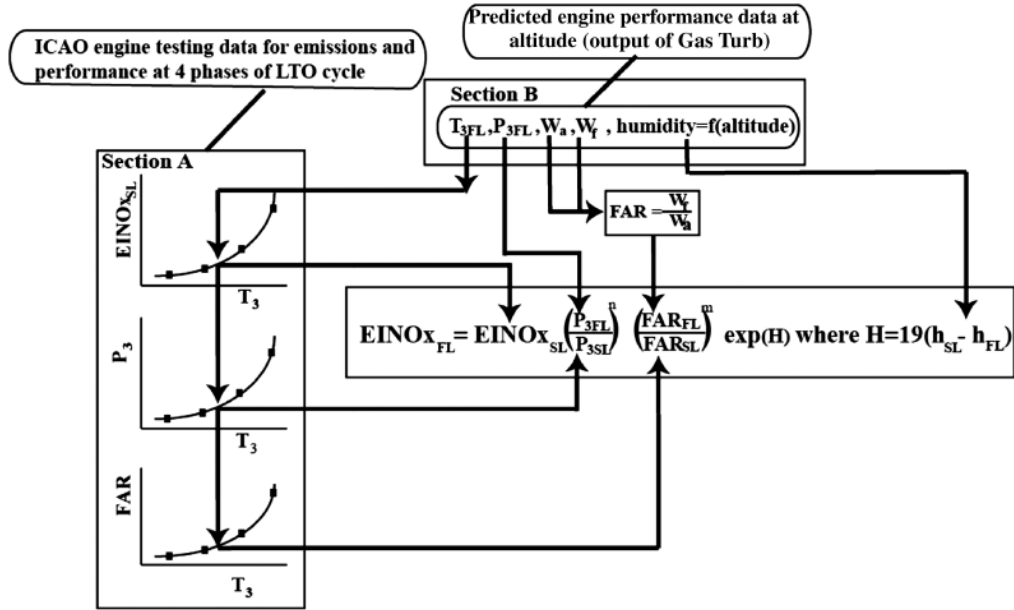


Figure 12: $P_3 - T_3$ Method Implementation for $EINO_x$ calculation [16]

In the fifth step, the sea-level emission indices calculated in the fourth step are adjusted to flight conditions using the following equations:

$$EICO_{Alt} = EICO_{SL} \left(\frac{P_{3SL}}{P_{3Alt}} \right)^x \left(\frac{FAR_{SL}}{FAR_{Alt}} \right)^z \quad (4.1)$$

$$EIHC_{Alt} = EIHC_{SL} \left(\frac{P_{3SL}}{P_{3Alt}} \right)^x \left(\frac{FAR_{SL}}{FAR_{Alt}} \right)^z \quad (4.2)$$

$$EINOx_{Alt} = EINOx_{SL} \left(\frac{P3_{Alt}}{P3_{SL}} \right)^Y e^H \left(\frac{FAR_{Alt}}{FAR_{SL}} \right)^Z \quad (4.3)$$

The exponents of Y and X are engine/combustor specific and are empirically derived by the manufacturers. The value for the Y exponent has been seen to range between 0.2 and 0.5 in rig and engine tests. Published empirical data would suggest an exponent of 0.4, while theory would suggest 0.5. The value of the X exponent is assumed to be 1.0. The value of the Z exponent is effectively 0 for conventional rich front-end single annular combustors, and so this term drops out of the equations.

The NOx equation includes a humidity factor e^H , where $H = 19(h_{SL} - h_{FL})$, because moisture in humid air entering the engine core and combustor reduces the peak flame temperature and NOx formation rate.

To effectively implement this method, it is necessary to have access to the proprietary performance model of the engine, which is often unavailable. Here is where the Boeing Fuel Flow Method Two finds its application, offering a method based on the most commonly available non-proprietary data of engine power settings.

4.1.3 Boeing Fuel Flow Method 2

The Fuel Flow Method is derived from the $P_3 - T_3$ method to overcome the problem of the availability of proprietary models and data to perform a chemical emission estimation analysis in a reference mission. The method is grounded on available data coming from the ICAO emission databank, and on the value of the fuel flow rate during the mission path.

The $P_3 - T_3$ method determines the emission index using the T_3 at flight altitude to look up an EI at sea level, and then corrects it by applying a pressure correction.

The idea of a "fuel flow method" comes from the fact that the emission indices at sea level are publicly known for certified engines as a function of fuel flow rate; fuel flow can be known from the engine power setting, and in the end, it can be correlated to T_3 . Finally, to implement the method, it is necessary to develop a pressure-correction formulation based on ambient or freestream pressure so that the method remains independent of proprietary manufacturer data.

BFFM2 is a method formulated by Martin et al. in 1994, available in Appendix D of Baughcum et al. [4]. The measured emission indices have to be

corrected to the conditions at flight altitude by using both altitude and ground level combustor operating conditions similar to the $P_3 - T_3$ method. These correction factors are derived by DuBois and Paynter [9] using thermodynamic relationships and energy balances.

The improved approach used for the second version of the method is based on an energy balance across the combustor that shows that there exists a fuel flow correlation that will result in the same T_3 at sea level as at flight conditions. It can be shown that the correlation essentially represents the difference in airflow rates through the combustor between sea level and flight conditions. Multiplying the fuel flow rate correlation factor by the engine fuel flow rate at altitude flight condition, the output is the equivalent sea-level fuel flow that would result in the same T_3 as at altitude.

The following section will explain the equations and reasoning behind the implementation of the method.

Assuming the compression process between freestream and combustor inlet is isentropic and using total quantity:

$$\frac{T_3}{T_1} = \left(\frac{P_3}{P_1}\right)^{\frac{\gamma-1}{\gamma}} \quad (4.4)$$

Writing the equation at sea level and flight level conditions:

$$T_{3FL} = T_{1FL} \left(\frac{P_{3FL}}{P_{1FL}}\right)^{\frac{\gamma-1}{\gamma}} \quad T_{3SL} = 288.15 \left(\frac{P_{3SL}}{101325}\right)^{\frac{\gamma-1}{\gamma}} \quad (4.5)$$

At the moment that in the $P_3 - T_3$ method $T_{3FL} = T_{3SL}$:

$$T_{1FL} \left(\frac{P_{3FL}}{P_{1FL}}\right)^{\frac{\gamma-1}{\gamma}} = 288.15 \left(\frac{P_{3SL}}{101325}\right)^{\frac{\gamma-1}{\gamma}} \quad (4.6)$$

That can be rewritten as:

$$\frac{P_{3FL}}{P_{3SL}} = \frac{\delta_1}{\theta_1^{\frac{\gamma}{\gamma-1}}} \quad \text{where} \quad \theta_1 = \frac{P_{1FLtotal}}{101325}, \quad \delta_1 = \frac{T_{1FLtotal}}{288.15} \quad (4.7)$$

From the compressible flow function relationships for total to static pressure and temperature ratios, it is possible to write:

$$\beta = 1 + \frac{\gamma-1}{2} M^2 \quad (4.8)$$

And rewrite 4.7 as:

$$\frac{P_{3FL}}{P_{3SL}} = \frac{\delta_{amb}\beta^{\frac{\gamma}{\gamma-1}}}{(\theta_{amb}\beta)^{\frac{\gamma}{\gamma-1}}} \quad \text{where} \quad \delta_{amb} = \frac{P_{1FLstatic}}{101325}, \quad \theta_{amb} = \frac{T_{1FLstatic}}{288.15} \quad (4.9)$$

For $\gamma = 1.4$:

$$\frac{P_{3FL}}{P_{3SL}} = \frac{\delta_{amb}}{\theta_{amb}^{3.5}} \quad (4.10)$$

An equivalent dissertation can be done assuming a polytropic compression from the freestream to the combustor inlet:

$$\frac{T_3}{T_1} = \left(\frac{P_3}{P_1}\right)^{\frac{\gamma-1}{\gamma\eta_p}} \quad (4.11)$$

Which leads to:

$$\frac{P_{3FL}}{P_{3SL}} = \frac{\delta_{amb}}{\theta_{amb}^{\frac{\gamma\eta_p}{\gamma-1}}} \quad (4.12)$$

For $\gamma = 1.38$ and $\eta_p = 90\%$:

$$\frac{P_{3FL}}{P_{3SL}} = \frac{\delta_{amb}}{\theta_{amb}^{3.3}} \quad (4.13)$$

In the end, a small empirically derived modification was made to the exponent of δ_{amb} to better collapse the data and results in the following pressure correction equation:

$$\frac{P_{3FL}}{P_{3SL}} = \frac{\delta_{amb}^{1.02}}{\theta_{amb}^{3.3}} \quad (4.14)$$

Finally, this equation can be substituted into the $P_3 - T_3$ reference emission indices correction equations resulting in:

$$EICO_{FL} = EICO_{SL} \left(\frac{\theta_1^{3.3}}{\delta_1^{1.02}} \right)^X \quad (4.15)$$

$$EIHC_{FL} = EIHC_{SL} \left(\frac{\theta_1^{3.3}}{\delta_1^{1.02}} \right)^X \quad (4.16)$$

$$EINO_{xFL} = EINO_{xSL} \left(\frac{\delta_1^{1.02}}{\theta_1^{3.3}} \right)^Y e^H \quad (4.17)$$

The exponents X and Y are the same that would be used in the P3-T3 method and depend on the engine. If information about the engine is not available, the default values to be used are X=1.0 and Y=0.5.

In the formulation for the correction of EINOx e^H appears: H is a humidity

correction term, which is necessary because humid air brings additional moisture into the engine core and combustor, reducing the peak flame temperature and consequently NOx emissions. The calculation of H according to Boeing is performed as follows:

$$H = -19(\omega - 0.00634) \quad (4.18)$$

$$\omega = \frac{0.62197058\Phi P_V}{P_{amb} - \Phi P_V} \quad (4.19)$$

Where ω is the specific humidity, Φ is the relative humidity, P_V is the saturation vapour pressure and P_{amb} is the inlet ambient pressure.

To implement the method, it is necessary to carry out the fuel flow rate correction. Applying an energy balance across the combustor leads to:

$$\eta_b W_f LHV = (W_f + W_a) C_p (T_4 - T_3) \quad (4.20)$$

Since the fuel flow rate is typically less than 2% of the airflow rate, it is possible to assume that the fuel and air are both at the same temperature T_3 and that they have the same specific heats, so the equation becomes:

$$\eta_b W_f LHV = W_a C_p (T_4 - T_3) \quad (4.21)$$

Since $P_3 - T_3$ method assumes that T_3 and T_4 do not change from sea level to flight level conditions, it can be asserted:

$$W_{fSL} = W_{fFL} \frac{W_{aSL}}{W_{aFL}} \frac{\eta_{bFL}}{\eta_{bSL}} \quad (4.22)$$

The airflow rate into the combustor at sea level is:

$$W_{aSL} = \sqrt{\frac{\gamma}{R}} \frac{P_{3SL}}{\sqrt{T_{3SL}}} M \left(\frac{1}{1 + \frac{\gamma-1}{2} M^2} \right)^{\frac{\gamma+1}{2(\gamma-1)}} \quad (4.23)$$

The same equation can be written at flight level, and since the combustor exit is choked, and the total temperatures T_3 and T_4 are assumed constant during the flight $f(M_3)_{SL} = f(M_3)_{FL}$ where $f(M_3) = M \left(\frac{1}{1 + \frac{\gamma-1}{2} M^2} \right)^{\frac{\gamma+1}{2(\gamma-1)}}$.

Substituting these expressions in the equation 4.22:

$$W_{fSL} = W_{fFL} \frac{P_{3SL}}{P_{3FL}} \frac{\eta_{bFL}}{\eta_{bSL}} \quad (4.24)$$

Relating the burner efficiency η_b to the fuel to air ratio by the equation 4.21, the last equation becomes:

$$W_{fSL} = W_{fFL} \frac{P_{3SL}}{P_{3FL}} \frac{\left(\frac{W_f}{W_a}\right)_{SL}}{\left(\frac{W_f}{W_a}\right)_{FL}} = W_{fFL} \frac{\theta_{amb}^{3.5}}{\delta_{amb}} \frac{\left(\frac{W_f}{W_a}\right)_{SL}}{\left(\frac{W_f}{W_a}\right)_{FL}} \quad (4.25)$$

It is allowable to find a relationship between fuel to air ratio and combustor inlet temperature T_3 using the standard non-dimensional analysis parameters:

$$T_{3SL} = \frac{T_{3FL}}{\theta_1} \quad \left(\frac{W_f}{W_a}\right)_{SL} = \frac{\left(\frac{W_f}{W_a}\right)_{FL}}{\theta_1} \quad (4.26)$$

The corrected fuel to air ratio plotted as function of the corrected T_3 must be fitted with a power function of this form:

$$\frac{\left(\frac{W_f}{W_a}\right)_{FL}}{\theta_1} = k \left(\frac{T_{3FL}}{\theta_1}\right)^X \quad (4.27)$$

This equation, expressed for both sea-level and flight-level conditions and suitably manipulated, leads to:

$$\left(\frac{W_f}{W_a}\right)_{SL} = \left(\frac{W_f}{W_a}\right)_{FL} \theta_1^{X-1} \quad (4.28)$$

Which can be insterted in equation 4.25:

$$W_{fSL} = W_{fFL} \frac{\theta_{amb}^{3.5}}{\delta_{amb}} \theta_1^{X-1} \quad (4.29)$$

To avoid requiring engine-specific exponents, a simple quadratic relationship is assumed by setting $X = 2$.

Using the compressible-flow relations for total to static pressure and temperature $\theta_1 = \theta_{amb}(1 + \frac{\gamma-1}{2}M^2)$ and assuming $\gamma = 1.4$ the equation 4.29 becomes:

$$W_{fSL} = W_{fFL} \frac{\theta_{amb}^{3.5}}{\delta_{amb}} \theta_{amb}(1 + 0.2M^2) \quad (4.30)$$

According to perturbation theory $e^{0.2M^2} \approx (1 + 0.2M^2)$, so the final equation that is used in the method is:

$$W_{fSL} = W_{fFL} \frac{\theta_{amb}^{4.5}}{\delta_{amb}} e^{0.2M^2} \quad (4.31)$$

To summarize, the steps required to implement the method are:

1. Retrieve emission indices from the ICAO Emissions Databank;
2. Determine the aircraft's mission profile: altitude, ambient temperature, pressure, density, Mach number, and fuel flow;
3. Compute sea-level fuel flow from flight-level fuel flow using the correlation formula;
4. Fit a power law relating ICAO emission indices to sea-level fuel flow, and apply it across all mission points;
5. Calculate flight-level emission indices from the sea-level values obtained in the previous step.

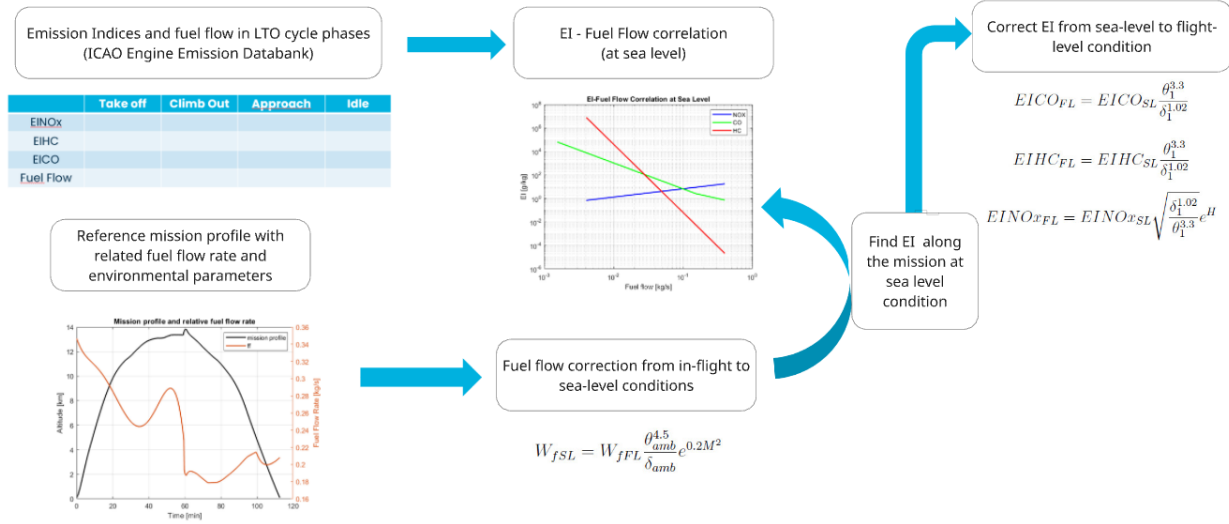


Figure 13: Boeing Fuel Flow Method Two Implementation

4.2 Local air quality impact assessment methods

Since the late 1970s, ICAO has worked to reduce the effect of aviation emissions on the air surrounding airports. The technical limits are set out in Annex 16, Volume II, which details permissible aircraft-engine pollutants and comes with extensive guidance [20].

ICAO's local-air-quality provisions regulate liquid-fuel venting, smoke (soon to be covered by the nvPM standard), and the key exhaust gases from jet engines: hydrocarbons, nitrogen oxides, and carbon monoxide.

At a more local level, some national agencies around the world have increased

their interest for the aviation sector’s impact on air quality near airports. In this regard, several research studies have been conducted, and low-to-high fidelity models and tools have been developed to address the problem of pollutant concentrations near airports that may harm the inhabitants of those areas. For example, the American Meteorological Society (AMS) and U.S. Environmental Protection Agency (EPA) developed the AERMOD model, while Ingenieurbüro Janicke, on behalf of the German Federal Environmental Agency (Umweltbundesamt) developed AUSTAL200 dispersion model.

Dispersion modeling is a fundamental process for air quality regulation. It enables the simulation of gas and particle dispersions and the prediction of pollutant concentrations in the atmosphere in a much more cost- and time-effective manner than traditional field measurements.

The origins of dispersion modeling lie in analytical models. The formulations of these models can follow either the Eulerian or the Lagrangian approach, but both allow the definition and description of the physics underlying dispersion phenomena and lead to the definition of more complex models.

This section will first provide an overview of analytical models, followed by an introduction to the most commonly used dispersion tools, both commercial and open-source.

4.2.1 Analytical dispersion models

A dispersion model is used to estimate how much of a pollutant will be present at ground level by combining data on the emission itself with information on atmospheric conditions.

In the literature different types of dispersion models are available, from simple box type models to complex fluid-dynamics models, and their suitability depends to scale, complexity of the environment and concentration parameters.

Box Model

The simplest dispersion algorithm treats the airshed as a rectangular *box* in which the pollutant is perfectly mixed. A transient mass balance over this control volume gives

$$\frac{d(CV)}{dt} = Q A + u C_{\text{in}} W H - u C W H, \quad (4.32)$$

where

- Q = pollutant emission rate per unit area;
- C = average pollutant concentration inside the box;
- V = volume of the box;
- C_{in} = concentration of the incoming air;
- A = horizontal area of the box;
- u = wind speed normal to the inflow face;
- W = effective width of the inflow face;
- H = mixing height;

Although straightforward, this approach presumes the contaminant is uniformly distributed throughout the airshed and is therefore best suited for estimating *average* concentrations over extensive areas.

Gaussian Model

The Gaussian diffusion model is widely applied in atmospheric studies to estimate the movement and concentration of air pollutants. This approach assumes that pollutants spread in the atmosphere according to a normal (Gaussian) distribution. It is grounded in the idea that the dispersion of substances follows a predictable pattern based on the Gaussian function. Such models are derived as analytical solutions to the gradient transport equation (Eq. 4.33), assuming steady wind conditions and stable turbulent flow.

$$\frac{\partial \bar{C}}{\partial t} + \bar{u} \frac{\partial \bar{C}}{\partial x} = \frac{\partial}{\partial x} \left(K_x \frac{\partial \bar{C}}{\partial x} \right) + \frac{\partial}{\partial y} \left(K_y \frac{\partial \bar{C}}{\partial y} \right) + \frac{\partial}{\partial z} \left(K_z \frac{\partial \bar{C}}{\partial z} \right) \quad (4.33)$$

where, \bar{C} denotes the pollutant concentration, \bar{u} represents the average wind speed, while K_x , K_y , and K_z are the coefficients for turbulent diffusion along the x , y , and z axes, respectively.

For a uniform flow with homogeneous turbulence and a continuous point source, the solution of Eq. 4.33 results in [48]:

$$\bar{C}(x, y, z) = \frac{Q \exp \left\{ -\frac{\bar{u}}{2K_x^{1/2}} \left[\left(\frac{x^2}{K_x} + \frac{y^2}{K_y} + \frac{z^2}{K_z} \right)^{1/2} - \frac{x}{K_x^{1/2}} \right] \right\}}{4\pi(K_x K_y K_z)^{1/2} \left(\frac{x^2}{K_x} + \frac{y^2}{K_y} + \frac{z^2}{K_z} \right)^{1/2}} \quad (4.34)$$

where Q represents the source strength or the emission rate.

By using the standard deviations of the Gaussian concentration distribution, σ_y and σ_z , and applying the slender plume approximation [3], Eq. 4.34 can be simplified into the well-known Gaussian plume equation:

$$C(x, y, z, H) = \frac{Q}{2\pi\bar{u}\sigma_y\sigma_z} \exp\left[-\frac{1}{2}\left(\frac{y}{\sigma_y}\right)^2\right] \cdot \left\{ \exp\left[-\frac{1}{2}\left(\frac{z-H}{\sigma_z}\right)^2\right] + \exp\left[-\frac{1}{2}\left(\frac{z+H}{\sigma_z}\right)^2\right] \right\} \quad (4.35)$$

With the symbols defined below:

- $C(x, y, z)$ = contaminant concentration at the downwind location (x, y, z)
- Q = mass-emission rate;
- u = mean wind speed at stack height;
- σ_y = horizontal dispersion parameter (standard deviation in y);
- σ_z = vertical dispersion parameter (standard deviation in z);
- H = effective release height (physical stack height plus plume rise);
- y = cross-wind distance from plume centreline;
- z = height above ground;

The plume's spread (quantified by σ_y and σ_z) depends on atmospheric stability, wind speed, surface heating, and cloud cover. Because these coefficients are simply the standard deviations of the Gaussian profile in the horizontal and vertical directions, larger values correspond to broader, more dilute plumes.

In the literature, several approaches exist to properly estimate these coefficients based on atmospheric stability. Hereafter are presented the Pasquill-Gifford formulation and the Green's formulation.

| Stability | a | b | c | $\epsilon(\%)$ |
|-----------|--------------|---------------|------------------|----------------|
| A | 209.6 | 0.8804 | -0.006902 | 0.37 |
| B | 154.7 | 0.8932 | -0.006271 | 0.29 |
| C | 103.3 | 0.9112 | -0.004845 | 0.27 |
| D | 68.28 | 0.9112 | -0.004845 | 0.18 |
| E | 51.05 | 0.9112 | -0.004845 | 0.21 |
| F | 33.96 | 0.9112 | -0.004845 | 0.25 |

Figure 14: Pasquill-Gifford σ_y formulation coefficients [7]

Figure 14 reports the least squares coefficients a , b , and c for the Pasquill-Gifford σ_y formulation, which has the following form:

$$\sigma_y = ax^{b+c \ln x} \quad (4.36)$$

where x is the downwind distance in kilometers (km), and σ_y is the lateral dispersion parameter in meters (m).

The ISC model is a more accurate representation of Pasquill-Gifford sigmas which has been developed for the Environmental Protection Agency, where:

$$\sigma_y = 465.12x \tan[0.01745)a - b \ln(x)] \quad (4.37)$$

The same can be applied to σ_z , leading to:

| Stability | a | b | c | $\epsilon(\%)$ |
|-----------|--------------|---------------|-----------------|----------------|
| A | 417.9 | 2.058 | 0.2499 | 5.05 |
| B | 109.8 | 1.064 | 0.01163 | 1.75 |
| C | 61.14 | 0.9147 | 0.0 | 0.01 |
| D | 30.38 | 0.7309 | -0.03200 | 1.87 |
| E | 21.14 | 0.6802 | -0.04522 | 0.71 |
| F | 13.72 | 0.6584 | -0.05367 | 1.15 |

Figure 15: Pasquill-Gifford σ_z formulation coefficients [7]

Where

$$\sigma_z = ax^{b+c \ln x} \quad (4.38)$$

Another valuable formulation reperible in the literature is Green's formulation [15]:

$$\begin{cases} \sigma_y(x) = \frac{k_1 x}{[1+(\frac{x}{k_2})]^{k_3}} \\ \sigma_z(x) = \frac{k_4 x}{[1+(\frac{x}{k_2})]^{k_5}} \end{cases} \quad (4.39)$$

Where the k_i coefficients are reported in the Figure below.

| Classe di Stabilit  | K ₁ | k ₂ | k ₃ | k ₄ | k ₅ |
|---------------------|----------------|----------------|----------------|----------------|----------------|
| A | 0.2500 | 927 | 0.189 | 0.1020 | -1.918 |
| B | 0.2020 | 370 | 0.162 | 0.0962 | -0.101 |
| C | 0.1340 | 283 | 0.134 | 0.0722 | 0.102 |
| D | 0.0787 | 707 | 0.135 | 0.0475 | 0.465 |
| E | 0.0566 | 1070 | 0.137 | 0.0335 | 0.624 |
| F | 0.0370 | 1170 | 0.134 | 0.0220 | 0.700 |

Figure 16: Green’s formulation coefficients

The Gaussian approach is valid under the hypothesis of uniformly mixed emitted material within the plume, and no strong chemical transformations occur during transport.

To apply a Gaussian formulation, the following conditions are generally imposed:

- The concentration field in any cross-section follows a normal (Gaussian) distribution;
- The emission rate Q is steady and continuous;
- Mean wind speed and direction remain uniform over the domain of interest;
- The ground behaves as a perfectly reflecting surface for the plume;
- The surrounding terrain is essentially flat (no significant obstructions or barriers).

Ambient air is gradually entrained into the jet, so the plume diameter enlarges with downwind distance. Momentum and buoyancy together force the gases to rise; this *plume rise* elevates the contaminants above the physical stack height. The *effective stack height* is therefore

$$H = h_s + \Delta h \quad (4.40)$$

where h_s is the physical stack height and Δh is the incremental rise to the centre-line of the plume.

Briggs (1969) [6] correlations for calculating the incremental rise of the plume due to momentum and buoyancy are:

$$\Delta h = \frac{1.6 F^{1/3} x^{2/3}}{\bar{u}}, \quad F = \frac{g V}{\pi} \frac{T_s - T_a}{T_s} \quad (4.41)$$

- Δh = plume rise above the stack tip;
- x = downwind distance from the stack;
- \bar{u} = mean wind speed at stack height;
- F = buoyancy flux;
- g = acceleration of gravity;
- V = volumetric flow rate of the stack gas;
- T_s = stack-gas temperature;
- T_a = ambient-air temperature.

Gaussian Puff Model

Puff models represent a continuous plume as a number of discrete packets of pollutant material. Most puff models (e.g. Ludwig et al., 1977, van Egmond and Kesseboom, 1983; Peterson, 1986) evaluate the contribution of a puff to the concentration at a receptor by a 'snapshot' approach. For every step time of the simulation, each puff is frozen, and the pollutant concentration due to it is evaluated; the puff is then allowed to evolve (it can move, change size, or modify its strength) until the next time step. In the end, the total concentration at a defined receptor is the sum of the contribution of all nearby puffs averaged for all sampling steps within the basic time step [39].

The well-known drawback of the puff approach is the need to release many puffs to adequately represent a continuous plume. Moreover, it has been shown that if the distance between puffs exceeds a maximum of approximately $2\sigma_y$, inaccurate results may occur. Hence, the snapshot sampling method requires a computationally expensive large number of puffs to be generated near the source.

The puff model is derived by relaxing the steady-state assumption from the Gaussian plume model to account for time-varying wind conditions and emission rates. Assuming the emission source is located at coordinate $(0, 0, z_0)$ the

concentration due to a single puff p from a point source is:

$$c_p(x, y, z, t) = \frac{m}{(2\pi)^{3/2}\sigma_y^2\sigma_z} \exp\left(-\frac{(x-ut)^2 + y^2}{2\sigma_y^2}\right) \times \left[\exp\left(-\frac{(z-z_0)^2}{2\sigma_z^2}\right) + \exp\left(-\frac{(z+z_0)^2}{2\sigma_z^2}\right) \right], \quad (4.42)$$

Where:

- m = mass of chemical species contained in puff p;
- σ_y, σ_z = dispersion coefficients;
- u = wind speed at the time the puff was released;

The overall concentration profile is the sum of the concentrations due to each puff:

$$c(x, y, z, t) = \sum_{p \in S_t} c_p(x, y, z, t), \quad (4.43)$$

where S_t is the set of all effective puffs occurred at time t .

It is importante to notice that the Gaussian puff model will provide the same concentration field as the Gaussian plume model if wind conditions are constant and a continuous plume is sufficiently well resolved by the number of puffs used in the approximation. The main benefit of the puff model is that introducing a time dependence allows the resolution of dynamics on shorter time scales.

This model forms the basis of the CALPUFF and SCIPUFF tools.

Simplified Gaussian Model

By solving the transport equation 4.33 for incompressible flow with isotropic and homogeneous diffusion coefficients, it is possible to derive a simplified expression [18]:

$$C(x, y, z, t) = \frac{Q}{(4\pi t)^{3/2} \sqrt{K_x K_y K_z}} \exp\left(-\frac{(x')^2}{4K_x t} - \frac{(y')^2}{4K_y t} - \frac{(z')^2}{4K_z t}\right) \quad (4.44)$$

Where:

- $C(x, y, z, t)$ = instantaneous concentration of pollutant [$\mu\text{g}/\text{m}^3$];
- Q = pollutant emission rate [$\mu\text{g}/\text{s}$];
- K_x, K_y, K_z = coefficients of atmospheric turbulence [m^2/s];

- t = time since the emission event begins [s];
- x', y', z' = coordinate of the point where concentration is considered;

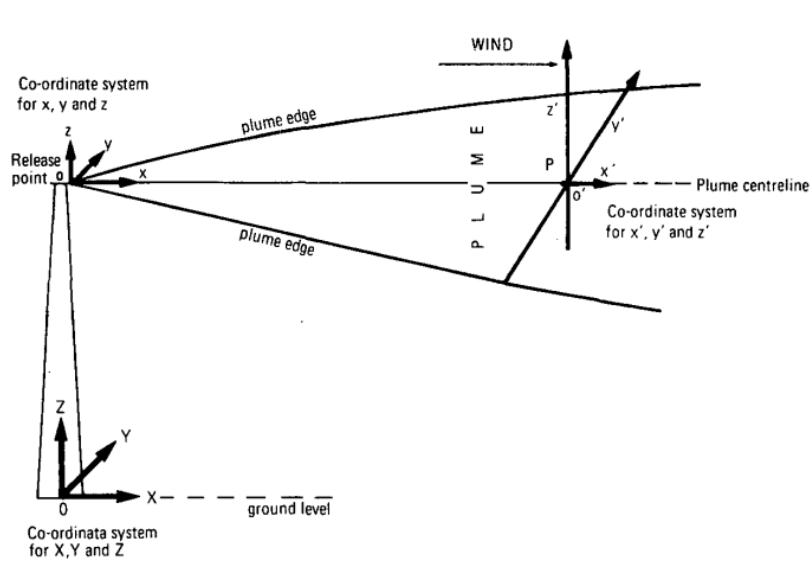


Figure 17: Gaussian plume evolution

The atmospheric dispersion model is based on the analytical solution of the advection-diffusion equation under the assumption of constant diffusion coefficients. However, to better reflect atmospheric conditions, the lateral and vertical diffusion parameters were treated as functions of distance, using the Pasquill-Gifford formulations. This approach effectively adapts the Gaussian solution to account for atmospheric turbulence and stability variations.

Accordingly, the dispersion parameters $\sigma_x, \sigma_y, \sigma_z$ were calculated using the formulations expressed above, and the coefficients of atmospheric turbulence are obtained by inverting the Turner formulation [41]:

$$\sigma_i = \frac{2K_i x}{u} \quad (4.45)$$

PolEmiCa Model

The PolEmiCa dispersion model is a semi-empirical model proposed by Kateryna Synylo and Oleksandr Zaporozhets [40].

The fundamental equation of the PolEmiCa model describes the instantaneous concentration of pollutants emitted by a moving source, such as a single exhaust event. It accounts for preliminary transport over a distance X_A , a rise to an altitude Δh , and dilution of the emitted pollutants with an initial standard

deviation σ_{0s} . The resulting concentration field is given by:

$$C(x, y, z, t) = \frac{Q \exp \left[-\frac{(x-x')^2}{2\sigma_y^2 + 4K_y t} - \frac{(y-y')^2}{2\sigma_z^2 + 4K_z t} \right]}{\left\{ 8\pi^3 [\sigma_x^2 + 2K_x t] [\sigma_y^2 + 2K_y t] \right\}^{1/2}} \cdot \frac{\left[\exp \left(\frac{(z-z'-H)^2}{2\sigma_z^2 + 4K_z t} \right) + \exp \left(\frac{(z+z'+H)^2}{2\sigma_z^2 + 4K_z t} \right) \right]}{[\sigma_z^2 + 2K_z t]^{1/2}} \quad (4.46)$$

Here, Q represents the emission rate, and K_x , K_y , K_z are the turbulent diffusion coefficients in the respective spatial directions.

The aircraft is modelled as a moving emission source. Therefore, its position at time t' is determined by the following expressions:

$$\begin{cases} x' &= x_0 + \mu_{PL} t' + 0.5a_{PL} t'^2 + u_W(t + t') \\ y' &= y_0 + \nu_{PL} t' + 0.5b_{PL} t'^2 \\ z' &= z_0 + \omega_{PL} t' + 0.5c_{PL} t'^2 \end{cases} \quad (4.47)$$

where:

- (x_0, y_0, z_0) = the initial coordinates of the emission source;
- $(\mu_{PL}, \nu_{PL}, \omega_{PL})$ = the velocity components of the source;
- (a_{PL}, b_{PL}, c_{PL}) = the acceleration components;
- $u_W(t + t')$ accounts for wind effects.

As in other dispersion models, the initial plume parameters are essential for accurately simulating its rise and spread. Parameters such as the plume rise height Δh (influenced by buoyancy), horizontal dispersion σ_y^2 , and vertical dispersion σ_z^2 are required as inputs.

4.2.2 Software and Tools

Given the growing interest in the assessment of local air quality impact of civil aviation, numerous software and tools have been developed by academies and agencies. Some of them are open source, while others require a purchasable licence.

This section aims to provide an overview of the available tools, which can serve as valuable resources for validating the implementation of the analytical models presented above and for conducting more complex dispersion analyses.

Open-ALAQs

Open-ALAQs is a modelling tool which estimates emissions from aircraft operation activities and various airport sources, together with those from on-airport infrastructure. It has been developed as a plug-in to an open-source geographic information system (QGIS). This strategic approach simplifies the definition of the various airport elements (e.g., taxiways, runways, buildings) and permits the visualisation of the spatial distribution of emission concentrations. Furthermore, it employs an open-source database (SQLite) and its open architecture allows its customization, making it compatible with other GISes and databases if required.

Among its functionalities, it is the performance of four-dimensional inventory emissions in which both the emissions from airport sources (i.e. aircraft operation activities) and the emissions from non-airport sources are calculated, summed up and displayed for analysis.

Once the inventory of the emissions is ready, it is feasible to calculate the pollutant concentrations at the airport and in its surrounding area over a determined period of time using dispersion modelling provided by AUSTAL2000. This is an open-source application which calculates the atmospheric dispersion of substances and odourants, and it is the official reference implementation of the instructions given in Appendix 3 of the German Regulation on Air Quality Control [26].

AUSTAL2000

AUSTAL2000 is a Lagrangian particle tracking air dispersion model that contains its own diagnostic wind field model (TALdia) developed by Janicke Consulting in Germany, under the commission of the German Federal Environment Agency (UBA). The model is capable of taking into account the influence of topography on the wind field and, therefore, on the dispersion of pollutants.

It is a steady-state dispersion model that is designed for long-term sources and continuous buoyant plumes. It is able to manage multiple point, area, volume, and line sources. In the model, dry deposition algorithms are implemented, and the conversion of NO to NO_2 is considered [17].

This tool is based on the Lagrangian dispersion model, which simulates the dispersion of air pollutants by utilizing a random walk process. This approach seems to be more accurate than the Eulerian one since it mimics the behaviour of particles. The direction and velocity of dispersion are estimated by wind

field vectors. Additionally, the vector of the turbulent velocity is randomly varied for every particle by using a Markov process. The random element varies with the intensity of turbulence. In the end, the concentration is calculated by counting the particles in a given volume.

The program AUSTAL2000 works non-interactively: all input data must be provided before the calculation in the project directory; when the program is started by the user, the calculation runs without further interaction and the results are stored to the project directory in a log file.

The calculation is carried out in a Cartesian coordinate system, where the x-axis runs from West to East and the y-axis from South to North. All length and coordinate specifications are in metres and refer to this coordinate system. For each project, the absolute position of the coordinate system's origin is set by the user, either in a Gauß-Krüger coordinate system (parameters `gx` and `gy`) or in a UTM coordinate system (parameters `ux` and `uy`). For practical reasons, the origin should be chosen close to the centre of emissions.

AUSTAL2000 requires the following input files:

- text file `austal2000.txt` with the main input parameters such as emission sources and emission strengths;
- A meteorological time series or a dispersion class statistics;

The minimum input files to run a simulation are the text file `austal2000.txt` and either a meteorological time series (AKTerm) or a dispersion class statistics (AKS). Both are provided, for example, by the National Weather Service (DWD in Germany). For more complex simulation the user must provide also:

- For time-dependent emission parameters: time series of parameter values in file `series.dmna`;
- For case-dependent parameters (in combination with a dispersion class statistics): for each parameter a DMNA file with the case-dependent values;
- For an automatic calculation of the roughness length `z0`: The register of roughness lengths in the main directory of AUSTAL2000;
- For complex terrain: The terrain profile of the applied calculation area in the file `zg00.dmna`.

The outputs of the calculations are provided in a log file (one for each substance evaluated).

LASPORT

LASPORT (LASAT for Airports) is a purchasable program system for the calculation of airport-related pollutant emissions and concentrations in the lower atmosphere [25].

It was developed in 2002 on behalf of the Federal German Airports Association (ADV) as a standard tool for emission and dispersion calculations.

It is the standard model tool of the German Airport Association and has been applied in various national and international projects (e.g., [22], [24], [21], [30]). It has been approved for use in ICAO/CAEP and complies with ICAO documents 9899 [19].

LASPORT provides the user with the following capabilities:

- Definition of source groups, emissions, and other parameters;
- Preparation and evaluation of journals with individual aircraft movements;
- Calculation of overall emissions for each source group and pollutant;
- Preparation, start, and control of the dispersion calculation with LASAT;
- Result analysis and graphical visualization.

This software is capable to taking into account emissions from the following sources:

- Aircraft traffic (LTO cycle divided into 6 phases);
- Auxiliary power units (APU), ground power units (GPU), engine start-ups;
- Ground support equipment (GSE) and de-icing;
- Motor traffic (airside and landside).

Along with them, the user can define other sources in form of point, line, and volume sources with individual emission strengths. Their specifications are inserted using the graphical interface or by formatted text files.

During the dispersion calculation, the dynamics of the engine exhaust from aircraft is accounted for by a directed exit velocity and turbulence characteristics, which are a function of aircraft group and LTO phase. For other source groups, thermal plume rise is covered parametrically based on the German

guideline VDI 3782 Part 3.

Linear conversion rates dependent on the atmospheric stability allow to model the chemical conversion of NO to NO_2 , according to the German standard VDI 3782 Part 1 [1].

It is also possible to carry out dispersion analysis in complex terrain and in the presence of buildings.

The dispersion of pollutants is calculated using weather data, usually collected every hour. This data includes:

- Wind speed
- Wind direction
- Atmospheric stability

With this information, the model calculates the three-dimensional concentration field of each trace substance averaged over successive time intervals of typically one hour. From these hourly results, the system produces:

- Long-term averages (over months or years)
- Short-term values (like 1-hour or 24-hour peaks), as required by EU regulations
- Pollutant deposition on the ground, including:
 - Dry deposition (without rain)
 - Wet deposition (with rain)
 - Total deposition (both combined)

The dispersion calculation is carried out with a subset of programs from the software package LASAT 3.4, which are integrated in the LASPORT software system.

The dispersion model LASAT (Lagrangian Simulation of Aerosol Transport) computes the transport of trace substances in the lower atmosphere (up to heights of about 2000 m) on a local and regional scale (up to distances of about 150 km). The dispersion is simulated utilizing a random walk process on a computer (Markov process) for a group of representative simulation particles. The advantages of this simulation method over other possible solutions are:

- The Lagrangian technique allows for a more accurate description of atmospheric dispersion in the near field of sources with respect to models based on the classical equation of diffusion;

- The method is not restricted to quasi-stationary dispersion situations, whereas Gaussian plume models are;
- It is possible to account for plume dynamics in detail;
- The user can give preference either to short calculation time or to high statistical accuracy by adjusting the number of simulation particles.

AERMOD

AERMOD is a steady-state plume model that incorporates air dispersion based on planetary boundary layer turbulence structure and scaling concepts, including treatment of both surface and elevated sources, and both simple and complex terrain [42].

It is labelled as steady-state since the meteorological conditions are assumed to be consistent and horizontally homogeneous during the modelling period of 1 hour. However, it can account for vertical variations of meteorological parameters in the planetary boundary layer.

AERMOD requires two regulatory input data processors that are:

- AERMET: it is a meteorological data preprocessor that incorporates air dispersion based on planetary boundary layer turbulence structure and scaling concepts;
- AERMAP: it is a terrain data preprocessor that incorporates complex terrain using USGS Digital Elevation Data.

AERMOD might be integrated with other non-regulatory components, which are:

- AEROSCREEN: a screening version of AERMOD;
- AERSURFACE: a surface characteristics preprocessor;
- BPIP PRIM: a multi-building dimensions program incorporating the GEP technical procedures for PRIME applications.

AERMOD has been designed to support the EPA's regulatory modeling programs, so the regulatory modeling options will be the default mode of operation for the model. Among these options, one can find the use of stack-tip downwash and a routine for processing averages in cases of calm winds or missing meteorological data. However, the model also incorporates various non-default

options such as suppressing the use of stack-tip downwash, deposition modeling, NO₂ conversion, special processing for low wind conditions, and disabling the date checking for non-sequential meteorological data files [43].

The model is capable of administering multiple sources, including point, volume area, open pit, and both buoyant and non-buoyant line source types. The buoyant line source algorithm from the Buoyant Line and Point Source (BLP) model [38] has been incorporated into the AERMOD model.

The effects of aerodynamic downwash due to nearby buildings on point source emissions and depositional effects on particulate emissions are considered by implementing proper algorithms in the model.

Source emission rates can be treated as constant throughout the considered period, or may be varied by month, season, hour-of-day, or other optional periods of variation. Variable emission rate factors may be specified for a single source or for a group of sources.

Regarding the receptors, the user has the capability of specifying multiple receptor networks in a single run and may also mix Cartesian grid receptor networks and polar grid receptor networks in the same run. In AERMOD there is no distinction between elevated terrain below release height and terrain above release height.

As illustrated above, AERMOD needs two types of meteorological input files which are generated by AERMET. These files are sequential ASCII files, and the model automatically recognizes the format generated by AERMET as the default format.

The outputs that AERMOD can provide are:

- Summaries of high values (highest, second highest, etc.) by receptor for each different combination of averaging period and source group;
- Summaries of overall maximum values for each averaging period and source group combination;
- Tables of concurrent values summarized by receptor for each combination of averaging period and source group, for each day of data processed. These "raw" concentration values may also be output to unformatted (binary) files.

Together with the output expressed above, AERMOD is capable of providing customizable output, for example it is possible to generate a file of (X, Y) coordinates and design values (e.g., the highest values at each receptor for a particular averaging period and source group combination) that can be easily

imported into many graphic plotting packages to generate contour plots of the concentration values.

Another useful functionality of AERMOD is that it can generate a file of all occurrences when a concentration value equals or exceeds a user-specified threshold, which can be extremely valuable for monitoring activities.

AERMOD dispersion estimations are based on the assumption that the concentration distribution is of Gaussian type. More specifically, under stable and neutral stratification with a Monin–Obukhov length (L) greater than 0, AERMOD assumes the concentration distribution to be horizontally and vertically of Gaussian type. During convective and neutral conditions with $L < 0$, AERMOD presumes a Gaussian distribution for the horizontal but a bi-Gaussian distribution for the vertical dimension [29].

The model also incorporates the three-plume concept for calculations in the convective boundary layer, which treats the emitted plume as if it came from three different sources:

- Direct source: it accounts for the part of the emissions that is carried directly to the ground;
- Indirect source: it accounts for the initial reflection at the mixing height and all subsequent reflections;
- Penetrated source: it accounts for the parts of the emissions that penetrate the elevated inversion and reenter it.

In the end downwash effects are calculated with the Plume Rise Model Enhancement (PRIME) algorithm.

CALPUFF

CALPUFF is an advanced non-steady-state meteorological and air quality modeling system. It is maintained and distributed by Lakes Environmental, and it has been listed by the U.S. Environmental Protection Agency (EPA) as an alternative model for assessing long-range transport of pollutants and their impacts on Federal Class I areas and for certain near-field applications involving complex meteorological conditions when the selection and use occur in agreement with the appropriate reviewing authority and approval by the EPA Regional Office [27].

CALPUFF modeling system consists of three main components which are:

- CALMET: it is a diagnostic three-dimensional meteorological model;
- CALPUFF: it is a Gaussian puff dispersion model with chemical removal, wet and dry deposition, complex terrain algorithms, building downwash, plume fumigation and other effects;
- CALPOST: it is a post-processing package for calculating time-averaged concentrations, deposition fluxes, and visibility impacts.

This is the minimum set to configure a simulation, but there exist several other processors that may be used to prepare geophysical data in many standard formats, meteorological data, and interfaces to other models.

Some of the applications that CALPUFF is capable of providing are:

- Near-field impacts in complex flow or dispersion situations;
- Long-range transport;
- Visibility assessments and Class I area impact studies;
- Criteria pollutant modeling, including application to State Implementation Plan (SIP) development;
- Secondary pollutant formation and particulate matter modeling;
- Buoyant area and line sources (e.g., forest fires and aluminum reduction facilities).

CALPUFF implements a multi-layer, multi-species non-steady-state Lagrangian Gaussian puff dispersion model which can simulate the effects of time- and space-varying meteorological conditions on pollutant transport, transformation, and removal. Furthermore, it contains modules for complex terrain effects, overwater transport, coastal interaction effects, building downwash, wet and dry removal, and simple chemical transformation[28].

5 Methodology

This section outlines the methodology used to estimate chemical emissions and assess the local air quality impacts of LTO cycle emissions.

The first step involved an extensive literature review to identify state-of-the-art methods for chemical emission estimation and air quality impact assessment. The findings are presented in Chapter 4 and guided the selection of the most appropriate approach.

Next, comprehensive research on White Knight Two, SpaceShipTwo, and their mission profiles was conducted to gather the data necessary for method application. The chosen case study is the suborbital A-to-A flight from Grottaglie Spaceport, which was previously simulated in ASTOS software (from liftoff to touchdown). To account for the ground roll acceleration and deceleration, both of which are not simulated in ASTOS, equations of motion and Raymer's formulations were applied.

Subsequent steps comprised applying the selected method to evaluate the chemical emissions over the reference mission and comparing the results with the FAA's Final Environmental Assessment for the Launch and Reentry of SpaceShipTwo Reusable Suborbital Rockets at the Mojave Air and Space Port[13].

Finally, to evaluate local air quality, a thorough review of analytical dispersion models and open-source tools was conducted. One model was selected, implemented, and validated against experimental measurements. Subsequently, a dispersion analysis of NO_x emissions during LTO cycle operations of the White Knight Two carrier was carried out using the LASPORT software system.

5.1 Chemical emissions assessment - LTO cycle

The evaluation of the emitted species during the phases of the ICAO LTO cycle has been carried out following the procedure outlined in ICAO Annex 16, Volume II [35].

The procedure can be summarised as:

1. Retrieve emission indices and fuel flow rate data for each LTO cycle phase from the ICAO Engine Emission Databank [12];
2. Calculate the emissions related to each phase;
3. Sum up the emissions to obtain the total LTO cycle emitted mass.

The formulation used to compute the emitted mass of a generic species j during a phase i in the second step is:

$$M_{ji} = EI_{ji} \cdot ff_i \cdot dt_i \quad (5.1)$$

5.2 Chemical emissions assessment - reference mission

The evaluation of the chemical species emitted by the WK2 aircraft during its nominal mission is performed using the Boeing Fuel Flow Method 2. To apply this method, it is necessary to know the mission trajectory (i.e., altitude and corresponding atmospheric conditions) and the fuel flow at each discrete point. A simulation of the mission was already implemented in ASTOS (Analysis, Simulation and Trajectory Optimization Software for Space Applications), which models the flight and outputs all relevant parameters at every instant. However, ASTOS models the flight only from lift-off to touchdown, so takeoff and landing ground rolls are excluded. To address this limitation, a simulation based on the equations of motion and the Raymer formulations [36] for estimating various aeromechanical parameters was implemented.

The steps followed to conduct the chemical emission assessment are summarized as follows:

1. Retrieve emission indices and fuel-flow data for each LTO cycle phase from the ICAO Emissions Databank [12].
2. Interpolate these data to correlate emission-index values with sea-level fuel flow.
3. Extract mission parameters (time, altitude, Mach, pressure, temperature, density, fuel flow) from the ASTOS simulation.
4. Integrate the takeoff and landing ground-roll equations using Raymer's formulation [36].
5. Adjust flight-level fuel flow to equivalent sea-level conditions at each mission instant.
6. Apply the correlation from step 2 to determine sea-level emission indices for each mission point.
7. Convert those sea-level emission indices back to flight-level conditions.

8. Compute total emissions along the trajectory by multiplying the emission index, the fuel flow, and the time interval between consecutive mission points.
9. Validate the results against the FAA's report [13].

The formulations used to convert between sea-level and flight-level conditions are those presented by DuBois in the description of Boeing Fuel Flow Method 2 [9] and are reported in Chapter 4.

5.2.1 Humidity correction factor

One possible criticality of the BFFM2 is the estimation of the exponent H , which appears in the equation that corrects $EINO_x$ at sea level to flight level conditions.

The humidity model is based on the assumption that humidity varies only with altitude. To simplify the calculations, relative humidity (RH) is assigned to the following altitude bands:

- $RH = 0.75$ for altitudes below 3000 m
- $RH = 0.66$ for altitudes between 3000 and 7000 m
- $RH = 0.60$ for altitudes between 7000 and 12000 m
- $RH = 0.70$ for altitudes between 12000 and 16000 m
- $RH = 0.50$ for altitudes above 16000 m

These bands were derived from the average values of several atmospheric models, the principal one being that shown in Figure 18.

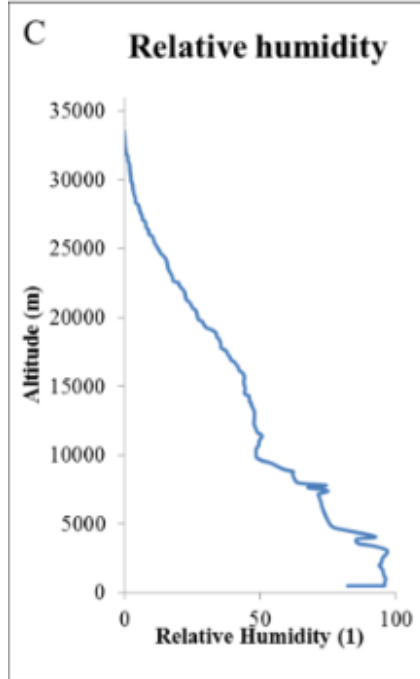


Figure 18: Profile of relative humidity [46]

5.2.2 ASTOS data collection

The reference mission was already simulated using the commercial software ASTOS by Astos Solution GmbH [8]. To perform the simulation, the required inputs are:

- The aerodynamic database containing drag and lift coefficients as a function of Mach and angle of attack;
- The propulsive database, containing thrust and fuel consumption as a function of Mach number, throttle and altitude;
- The vehicle's empty weight, payload and fuel mass;
- The mission phases that compose the desired trajectory.

The simulation output provides, at each mission instant, various pieces of information, including flight time, altitude, latitude, longitude, ambient temperature, pressure, density, Mach number, turbofan fuel-flow consumption, and aerodynamic and aeromechanical data.

Thus, the mission trajectory and all the information needed to implement the BFFM2 are available. However, minor adjustments may be necessary, since the simulation software has its limitations; the provided data must always be

critically analysed to verify their physical plausibility.

5.2.3 Takeoff and Landing ground-roll implementation methodology

Since ASTOS does not simulate the entire takeoff and landing phases, it is necessary to integrate the missing segments to have a better, comprehensive estimate of the emissions.

For what that concerns the takeoff, the simulation of the ground roll needs to be carried out. It includes two parts: the level ground roll and the ground roll during rotation to the angle of attack for liftoff.

The forces that act on the aircraft during the ground roll are lift, weight, thrust, drag, and rolling friction of the wheels. The last one can be expressed as a rolling friction coefficient μ multiplied by the effective weight acting on the wheels (W-L).

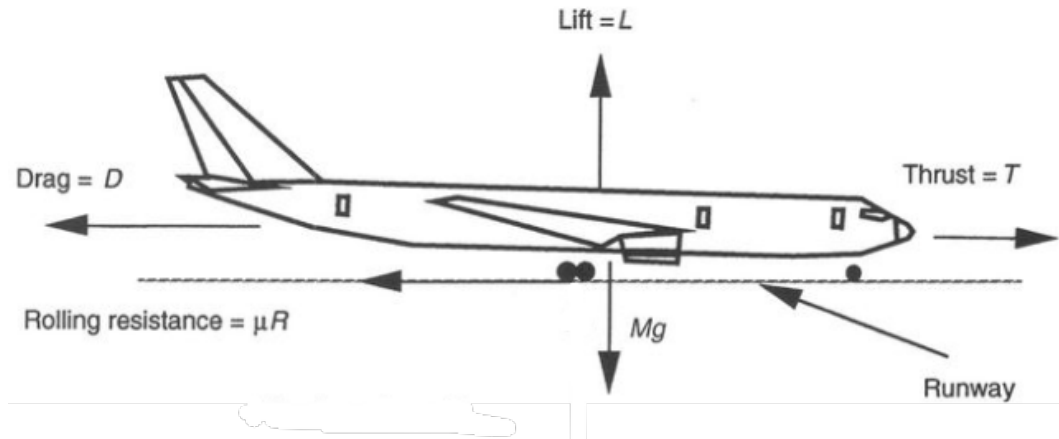


Figure 19: Forces acting during takeoff ground roll

A table presenting typical values of the rolling resistance coefficient (μ) for various surface conditions is provided in *Aircraft Design: A Conceptual Approach* [36].

| Surface | μ -typical values | |
|----------------------|-----------------------|-----------|
| | Rolling (brakes off) | Brakes on |
| Dry concrete/asphalt | 0.03–0.05 | 0.3–0.5 |
| Wet concrete/asphalt | 0.05 | 0.15–0.3 |
| Icy concrete/asphalt | 0.02 | 0.06–0.10 |
| Hard turf | 0.05 | 0.4 |
| Firm dirt | 0.04 | 0.3 |
| Soft turf | 0.07 | 0.2 |
| Wet grass | 0.08 | 0.2 |

Figure 20: Ground rolling resistance

By applying the equilibrium equation in the longitudinal direction, the acceleration can be expressed as:

$$\ddot{x} = \frac{g}{W}[T - D - \mu(W - L)] \quad (5.2)$$

By numerically integrating this equation using the explicit Euler method, the velocity and position can be obtained, thus yielding the total distance covered during this segment.

It is possible to implement a cycle, from null velocity to takeoff velocity, where $V_{TO} = 1.1V_{stall}$, but it requires evaluating the lift and drag of the aircraft for each integration step.

Lift and drag can be expressed in terms of the aerodynamics coefficient as:

$$L = \frac{1}{2}\rho V^2 S C_L \quad D = \frac{1}{2}\rho V^2 S C_D \quad (5.3)$$

Where $C_D = C_{D0} + kCL^2$.

Raymer's formulations [36] enable to properly estimate these coefficients and so to proceed with the numerical integration.

One can find:

$$C_{L_{maxflapped}} = C_{L_{maxclean}} + \Delta C_{L_{max}} \quad (5.4)$$

$$\Delta C_{L_{max}} = 0.92 * \Delta C_{L_{maxflap}} \frac{S_{flapped}}{S} \cos(\Lambda_{25}) \quad (5.5)$$

Where $S_{flapped}$ is the portion of the wing with flap and slat as shown in Figure 22, Λ_{25} is the swept angle at 25% of the wing chord and $\Delta C_{L_{maxflap}}$ depends on the type of flap and slat installed on the wing, and it is tabulated in Figure 21.













| | | $C_{L,max}$ | $\Delta C_{L,max}$ |
|------------------------------|---|-------------|--------------------|
| Clean Airfoil |  | 1,45 | - |
| Plain Flap |  | 2,25 | 0,80 |
| Single-Slotted Flap |  | 2,60 | 1,15 |
| Double-Slotted Flap |  | 2,80 | 1,35 |
| Split Flap |  | 2,40 | 0,95 |
| Double-Wing (Junkers) |  | 2,25 | 0,80 |
| Fowler Flap |  | 2,80 | 1,35 |
| Slat |  | 2,00 | 0,55 |
| Combinations: | | | |
| Plain Flap and Slat |  | 2,45 | 1,00 |
| Single-Slotted Flap and Slat |  | 2,70 | 1,25 |
| Double-Slotted Flap and Slat |  | 2,90 | 1,45 |
| Fowler Flap and Slat |  | 3,00 | 1,55 |

Figure 21: Maximum lift coefficient of profiles with different high-lift devices (based on data from Dubs 1987) [37]

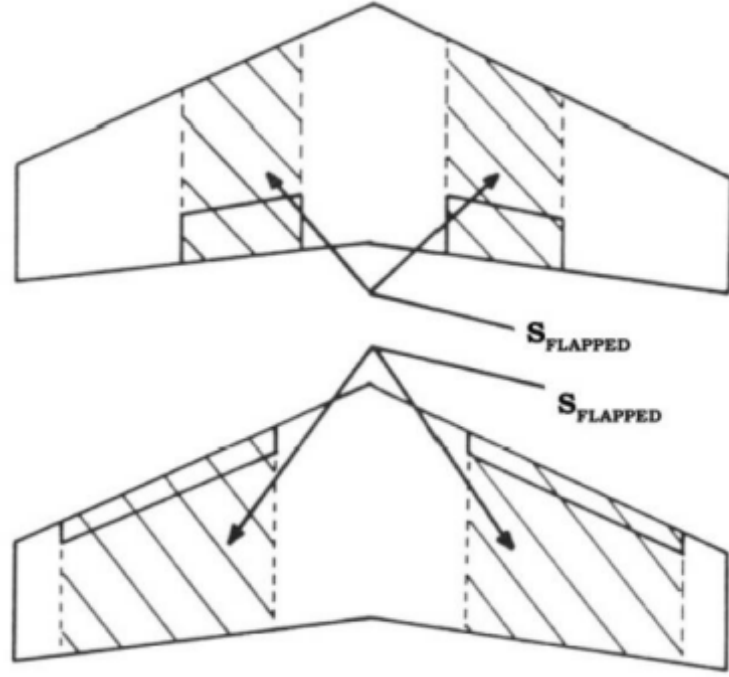


Figure 22: Flapped surface evaluation

Based on the CFD analysis previously conducted to generate the aerodynamic database for the ASTOS mission simulation, the zero-lift drag coefficient and the clean-configuration lift coefficient are supplied and their values are $C_{D0} = 0.0301$ and $C_{Lclean} = 1.3$ for WK2 in single configuration and $C_{D0} = 0.0367$ and $C_{Lclean} = 1.45$ in mated configuration.

For takeoff, the initial velocity is zero and the final velocity is V_{TO} . Since thrust varies during the ground roll, an average thrust value must be employed. Because the integration is carried out concerning the square of the velocity, the thrust to be used corresponds to that available at approximately 70% of V_{TO} (i.e. $V_{TO}/\sqrt{2}$).

The final segment of the ground-roll phase is the rotation, during which the aircraft pitches up to its liftoff attitude. For large aircraft, it is common to assume negligible acceleration (i.e. constant velocity) and a rotation duration of about 3 s. For smaller aircraft, such as the one under examination, the rotation typically lasts around 1 s, so $x_{rotation} = V_{TO} \cdot 1$.

Regarding the landing phase, the equation governing the ground roll is the same as for takeoff. It is necessary to account for weight loss due to fuel consumption; a typical assumption is to set it at 85% of MTOW.

After touchdown, the aircraft rolls freely for several seconds before the pilot applies the brakes. This distance is computed as $x_{rf} = V_{TD} \cdot 1$ under the same considerations used for the takeoff rotation distance.

The braking distance is determined by the same equation used for the takeoff ground roll, since the acting forces are the same. The integration takes place between an initial velocity of V_{TD} and a null final velocity.

The thrust term is the idle thrust, which is estimated from the fuel flow rates provided by ICAO for idle and for takeoff, assuming 100% thrust during takeoff. This leads to $T_{idle} = 0.125T_{to}$.

The rolling resistance must account for brake application: a typical value of μ under these conditions increases to 0.5 on a hard civil runway surface.

5.3 Air quality impact assessment

The evaluation of the air quality impact is divided into two parts:

- Calculation of the average concentration of NO_x in the engine plume during the takeoff using an analytic model;
- Simulation of the dispersion of NO_x during the LTO cycle using LAS-PORT.

5.3.1 Evaluation of NO_x average concentration in the engine plume

The average concentration of NO_x pollutants in the engine plume during the takeoff phase was evaluated using an analytical dispersion model derived from the solution of the transport equation and validated against experimental data. The spatio-temporal evolution of nitrogen-oxide (NO_x) concentrations is described with the analytic Gaussian simplified formulation $C(x, y, z, t)$ discussed in Chapter 4.

Employing this formulation enables a preliminary estimate of NO_x average dispersion during a period of time and provides a consistent baseline for comparison with numerical simulations and experimental data.

The applied formulation is:

$$C_{NO_x}(x, y, z, t) = \frac{Q_{NO_x}}{(4\pi t)^{3/2} \sqrt{K_x K_y K_z}} \exp\left(-\frac{(x-x')^2}{4K_x t} - \frac{(y-y')^2}{4K_y t} - \frac{(z-z')^2}{4K_z t}\right) \quad (5.6)$$

The atmospheric turbulence coefficients (K_i) were calculated from the dispersion parameters (σ_i) using Equation 4.45, while the dispersion parameters themselves were obtained using Green's formulations (Equation 4.39).

The dispersion parameters along the x and y axes were assumed to have the

same value.

The model was first validated by calculating the averaged concentration of NO_x during the takeoff phase and comparing it with experimental data reported in Kateryna Synylo and Oleksandr Zaporozhets' paper [40]. Indeed, the referenced paper reports the measured NO_x concentrations (averaged over 1 minute) measured by the NO_x analyzer in aircraft engine plume during take-off stage, and the relative calculated NO_x concentrations by the complex PolEmiCa model.

After that, the same procedure was applied to the WK2 and Dreamlifter engines, to compare their potential relative impact on the ground.

In this preliminary assessment, the emission source was considered static at a reference position, and the emission was assumed to be continuous over the period of interest, which was 1 minute, accordingly with what has been done in the literature.

The methodology applied for the evaluation of pollutant dispersion can be summarised in the following steps:

1. Define the position of the static, continuously emitting source;
2. Define the grid where pollutant concentrations will be calculated;
3. Define the emission rate: $Q = EINO_{x_{takeoff}} \cdot f_{takeoff}$;
4. Calculate σ_i using Green's formulations;
5. Calculate K_i using Turner's formulations;
6. Calculate the concentration at each point of the grid for every instant during the phase;
7. Calculate the average concentration over the entire phase duration for each point of the grid.

The spatial grid considered is 30 m wide in each direction and centered on the emission source, where the concentration values are the highest.

The model is capable of considering a continuous emitting source, and the step time used was 1 s.

5.3.2 WK2 LTO Cycle Dispersion Analysis Using LASPORT

The dispersion of NO_x pollutant during the LTO cycle's phases was investigated using the LASPORT tool.

As the software system is not open-source and the demo version only permits rerunning predefined examples, and given that the required simulations demanded advanced functionalities as described in [23] by Janicke Consulting, the simulations were therefore performed by the development team, to whom the necessary setup data were provided.

The aircraft movements were located at runway 35 of Taranto-Grottaglie Airport (LIBG).

The following cases were defined:

- Departure (take-off and climb) from runway 35 with head wind;
- Arrival (approach and ground roll) to runway 35 with head wind;
- Idle at a fixed position.

The three cases were prepared as three individual movements separated by about 2 hours. For each case, it is mandatory to specify:

- The resulting times-in-mode up to 895 m above ground level;
- The average NO_x emission rates for each segment (assuming 4 engines);
- Wind speed and direction at 10 m above ground;
- Surface roughness;
- Atmospheric stability class.

The times-in-mode up to 895 m above ground for each segment are calculated using Raymer's simulation for the takeoff and landing ground roll, and ASTOS data from liftoff to 895 m, and from that altitude down to touchdown.

Regarding the average NO_x emission rates for each segment, the values for idle, takeoff, and landing are taken from the ICAO Emissions Databank [12], while those for the climb and approach segments are averages of the emission index calculated using the Boeing Fuel Flow Method 2, from the beginning of the climb to 895 m, and from the beginning of the approach to touchdown.

The simulation is carried out under the assumption of a headwind of 3 m/s for both departure and arrival operations.

The surface roughness is defined as the height above the displacement plane at which the mean wind becomes zero when extrapolating the logarithmic wind speed profile downward through the surface layer. It depends on the terrain and its value has been chosen from the Table presented in Figure 23 reported

in the WMO Guide to Meteorological Instruments and Methods of Observation [47].

**Terrain classification from Davenport (1960) adapted by Wieringa (1980)
in terms of aerodynamic roughness length z_0**

| <i>Class index</i> | <i>Short terrain description</i> | <i>z_0 (m)</i> |
|--------------------|--|-----------------------------|
| 1 | Open sea, fetch at least 5 km | 0.0002 |
| 2 | Mud flats, snow; no vegetation, no obstacles | 0.005 |
| 3 | Open flat terrain; grass, few isolated obstacles | 0.03 |
| 4 | Low crops; occasional large obstacles, $x/H > 20$ | 0.10 |
| 5 | High crops; scattered obstacles, $15 < x/H < 20$ | 0.25 |
| 6 | Parkland, bushes; numerous obstacles, $x/H \approx 10$ | 0.5 |
| 7 | Regular large obstacle coverage (suburb, forest) | 1.0 |
| 8 | City centre with high- and low-rise buildings | ≥ 2 |

Figure 23: Surface Roughness Length [47]

The value selected for the simulation was 0.03, as the flight corridor for departure and arrival passes over open, flat terrain with few isolated obstacles. Finally, the atmospheric stability, describing the atmosphere's tendency to either promote or resist vertical motion, was set to neutral (class D).

The last three data serve to set the meteorology for the simulation, with the keys data expressed above the boundary layer profiles were set up according to the standard VDI 3783-8 [44]. Each movement was modelled as a moving source with time-dependent exhaust properties and emission rate, and the time resolution was 5s.

6 Chemical emissions estimation results

6.1 White Knight Two LTO cycle emissions

A significant initial quantitative metric for evaluating the aircraft's emissions and their impact on local air quality could be the emissions produced during the LTO cycle.

To properly evaluate them, it is possible to use the emission indices, expressed in grams of emitted species per kilogram of fuel burned, and multiply them by the fuel flow rate and the duration of each phase of the LTO cycle.

The emission indices of the proportional species, sourced from the literature [34], are reported below.

| Species | EI [g/kg] |
|---------|-----------|
| CO_2 | 3160 |
| H_2O | 1230 |
| SO_x | 0.8 |

Table 3: Emission Index proportional species [32]

The emission indices of the non-proportional species for each phase, along with the respective fuel flow rate, are reported in the table below and come from the ICAO Engine Emission Databank [2].

| Species | EI TO [g/kg] | EI Climb [g/kg] | EI App [g/kg] | EI Idle [g/kg] |
|---------|--------------|-----------------|---------------|----------------|
| CO | 0.83 | 1.06 | 4.08 | 38.21 |
| HC | 0 | 0 | 0.02 | 6.62 |
| NO_x | 16.74 | 14.06 | 8.03 | 3.65 |

Table 4: Emission Index LTO cycle non-proportional species

| | Take Off [kg/s] | Climb [kg/s] | Approach [kg/s] | Idle [kg/s] |
|----------------|-----------------|--------------|-----------------|-------------|
| Fuel flow rate | 0.360 | 0.299 | 0.124 | 0.045 |

Table 5: Fuel flow rate LTO cycle

The equation used to estimate the emissions of a general chemical species 'x' during a specific LTO cycle phase 'y' is:

$$Emission_{x-y} = EI_{x-y} \cdot \dot{m}_{fuel-y} \cdot duration_y \quad (6.1)$$

Table 6 shows the total LTO cycle emission of White Knight Two aircraft equipped with four turbofan PW308A. The same results are presented in Fig-

ures 24 and 25. For readability purposes, emissions are expressed in tons for the first two species and in kilograms for the remaining ones.

| Species | Take Off | Climb | Approach | Idle | Total |
|-------------|----------|-------|----------|--------|-------|
| CO_2 [t] | 0.191 | 0.499 | 0.376 | 0.847 | 1.913 |
| H_2O [t] | 0.074 | 0.194 | 0.146 | 0.345 | 0.760 |
| CO [kg] | 0.050 | 0.167 | 0.486 | 10.729 | 11.43 |
| HC [kg] | 0 | 0 | 0.002 | 1.859 | 1.861 |
| NO_x [kg] | 1.012 | 2.220 | 0.956 | 1.025 | 5.213 |
| SO_x [kg] | 0.048 | 0.126 | 0.095 | 0.225 | 0.495 |

Table 6: LTO cycle WK2 chemical emissions - four engines

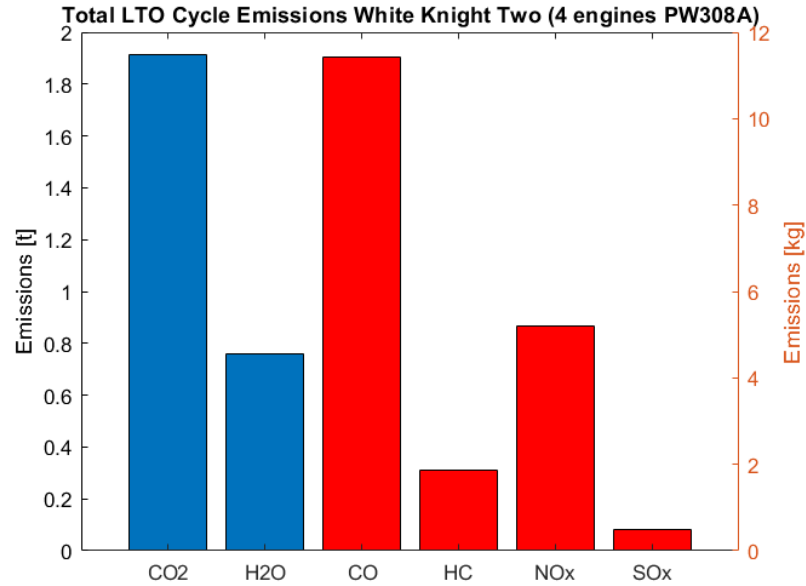


Figure 24: LTO emissions White Knight Two

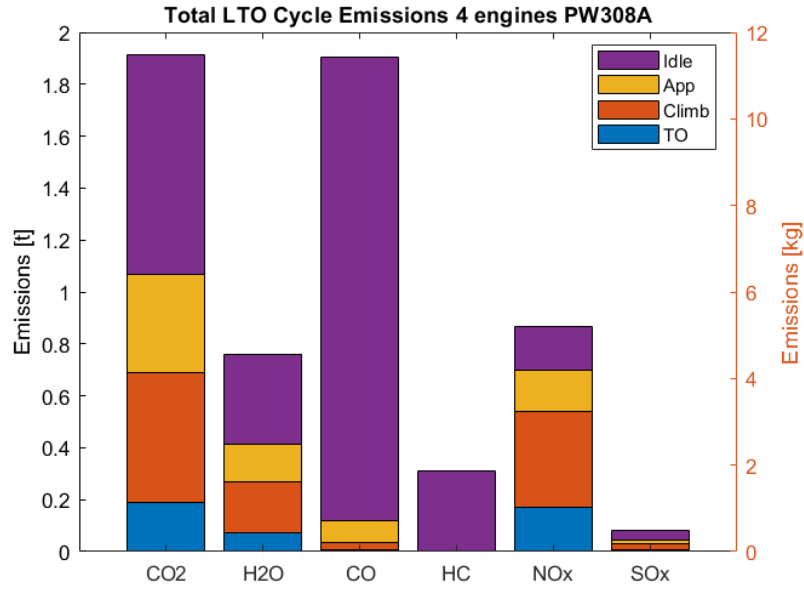


Figure 25: LTO emissions White Knight Two - phases insight

It is important to note that for CO_2 , H_2O , CO , SO_x , and HC , the idle phase is the worst, while for NO_x , the climb phase is the most critical due to the high power setting.

The results obtained can be compared with the LTO cycle emission evaluated in the FAA's report [2]:

| Species | CO_2 | H_2O | CO | NO_x | SO_x | HC |
|------------------|--------|--------|-------|--------|--------|------|
| Current [pounds] | 4218.4 | 1676.7 | 25.14 | 11.47 | 0.495 | 4.10 |
| FAA [pounds] | 4242 | 1685 | 27.09 | 11.05 | 1.74 | - |

Table 7: Comparison ICAO LTO cycle emission

We observe optimal correspondence between the results for both proportional and non-proportional species. The only exception is SO_x . As a proportional species, its emission index is not included in the ICAO Emission Databank; and since the other species show coherence, the discrepancy cannot be attributed to phase duration nor to fuel-flow rate. It therefore likely stems from the choice of emission index, which was sourced from the literature ([32]) but is not specific to this engine.

6.1.1 A comparison: LTO cycle emissions by Boeing 747 LCF Dreamlifter

Regarding the topic of social acceptance by the population bordering Grottaglie Airport, it may be interesting to compare the LTO cycle emissions of the analysed carrier WK2 with those of a recurrent flight of that airport, namely Boeing 747 LCF Dreamlifter. Indeed, with weekly cadence, Dreamlifter flights from Grottaglie to Charleston carry fuselage sections of the Boeing 787 Dreamliner.

Since the LTO cycle emissions are the most impactful for local air quality and consequently public opinion, it might be useful to make this comparison to demonstrate that A-to-A suborbital flight can perfectly integrate into the civil aviation panorama without disturbing local communities.

To calculate the LTO cycle emissions of the Boeing 747 LCF Dreamlifter, the same approach explained in Chapter 5 has been employed.

The Dreamlifter is a highly modified version of the Boeing 747-400 airliner, designed for transporting large aircraft components, and it is powered by 4 turbofan engines, model Pratt&Whitney PW4062, whose data are available in the ICAO Emission Databank [12] since it is certified.

Regarding the proportional species, the emission indices are the same reported in Table 3, while those of the non-proportional species are reported in the Table below.

| Species | EI TO [g/kg] | EI Climb [g/kg] | EI App [g/kg] | EI Idle [g/kg] |
|---------|--------------|-----------------|---------------|----------------|
| CO | 0.61 | 0.5 | 1.93 | 42.61 |
| HC | 0.08 | 0.07 | 0.09 | 10.86 |
| NO_x | 34.36 | 25.98 | 12.17 | 3.78 |

Table 8: Emission Index LTO cycle non-proportional species Dreamlifter

The fuel flow rate for each phase is:

| | Take Off [kg/s] | Climb [kg/s] | Approach [kg/s] | Idle [kg/s] |
|----------------|-----------------|--------------|-----------------|-------------|
| Fuel flow rate | 2.725 | 2.125 | 0.718 | 0.21 |

Table 9: Fuel flow rate LTO cycle Dreamlifter

The total ICAO LTO cycle emissions of the Boeing 747 LCF Dreamlifter are reported in Table 10. The same results are then expressed in the graphics below. For readability purposes, emissions are measured in tonnes for the first two species and in kilograms for the remaining ones.

| Species | Take Off | Climb | Approach | Idle | Total |
|-------------|----------|-------|----------|-------|-------|
| CO_2 [t] | 0.361 | 0.89 | 0.54 | 0.99 | 11.12 |
| H_2O [t] | 0.14 | 0.345 | 0.212 | 0.402 | 4.4 |
| CO [kg] | 0.07 | 0.14 | 0.33 | 13.96 | 58.01 |
| HC [kg] | 0.009 | 0.02 | 0.016 | 3.56 | 14.41 |
| NO_x [kg] | 3.93 | 7.29 | 2.097 | 1.238 | 58.22 |
| SO_x [kg] | 0.366 | 0.898 | 0.551 | 1.048 | 2.86 |

Table 10: LTO cycle Dreamlifter chemical emissions

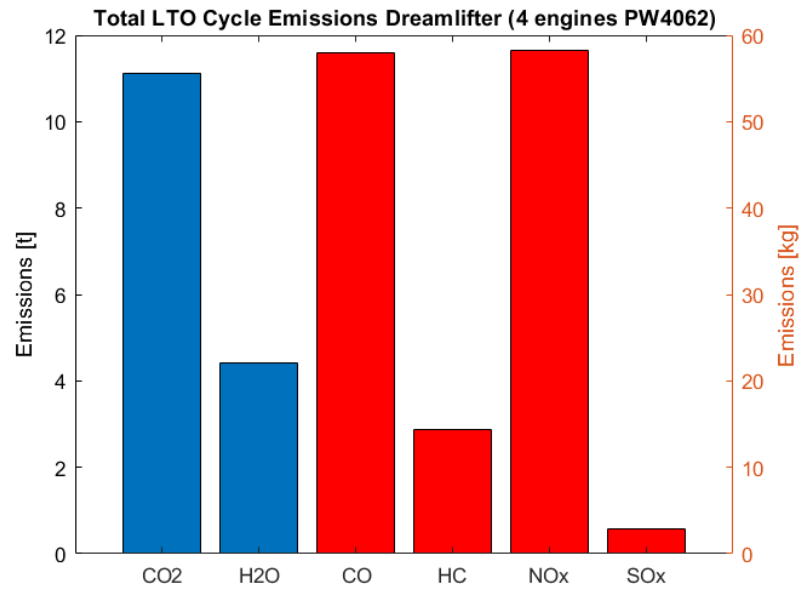


Figure 26: Total LTO cycle Emissions Dreamlifter

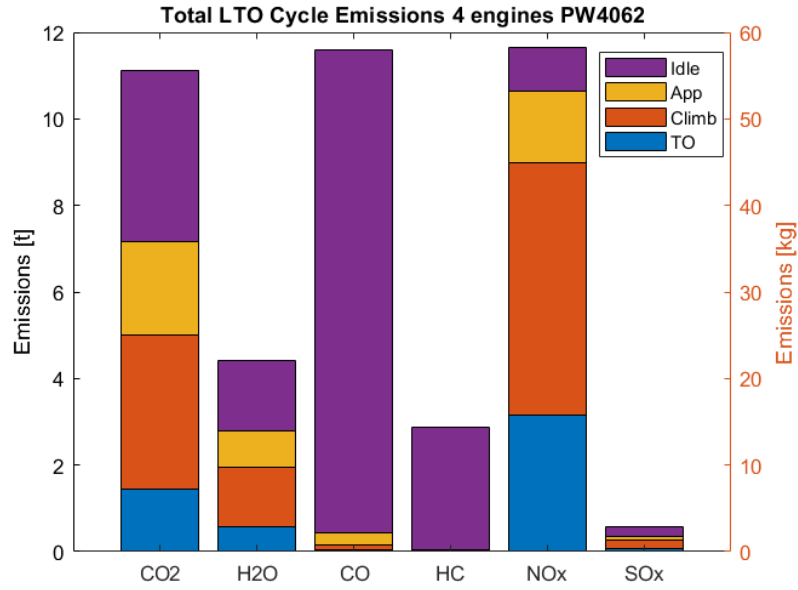


Figure 27: Total LTO cycle Emissions Dreamlifter - phases insight

The distributions of chemical species emissions during the phases are similar to those of WK2. These trends can be justified since the emissions are strictly related to the engine regime and consequently to the phase analysed. The idle phase is the worst for CO, CO₂ and H₂O while the climb phase is the gravest for NO_x.

Comparing the LTO cycle emissions of the two aircraft reveals that the Dreamlifter produces more chemical emissions than WK2. These evaluations could be fundamental to demonstrate to concerned people that the operational activities required for suborbital flights have a smaller impact on local air quality than current ongoing operations.

| Species | CO ₂ [t] | H ₂ O [t] | CO [kg] | NO _x [kg] | SO _x [kg] | HC [kg] |
|-------------|---------------------|----------------------|---------|----------------------|----------------------|---------|
| Dreamlifter | 11.12 | 4.4 | 58.01 | 58.22 | 2.86 | 14.41 |
| WK2 | 1.91 | 0.760 | 11.43 | 5.21 | 0.495 | 1.86 |

Table 11: Comparison ICAO LTO cycle emission Dreamlifter vs. WK2

6.2 White Knight Two reference mission emissions

The following section will present the results obtained applying the methodology illustrated in Chapter 5 to estimate the chemical emissions of WK2 during a nominal mission from and to Grottaglie airport.

The first step is to correlate the emission indices reported in the ICAO Emission Databank [12] for the reference PW308A engine with the fuel flow rate.

The results are shown in the bi-logarithmic graph below.

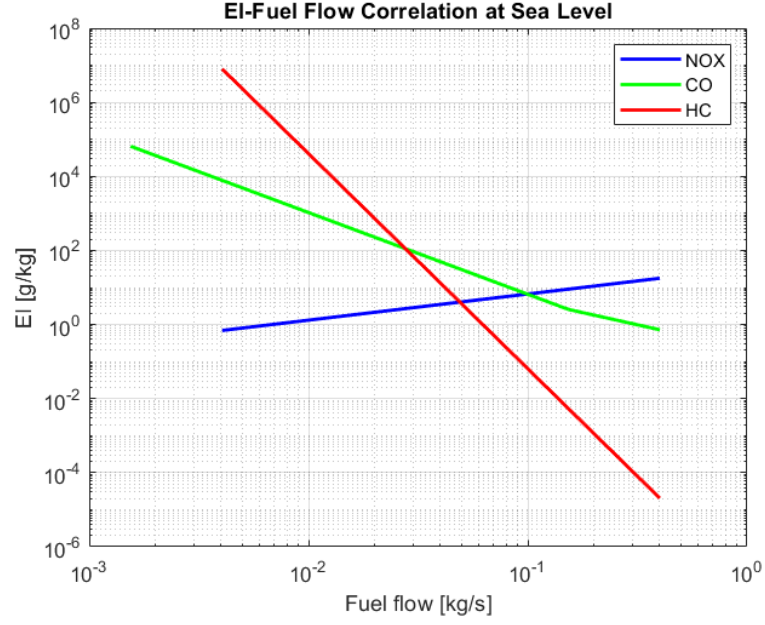


Figure 28: EI correlation with fuel flow rate

The interpolation results in the following expression:

$$EINO_x(y) = 33.922y^{0.7064} \quad (6.2)$$

$$EIHC(y) = 10^{-7}y^{-5.8069} \quad (6.3)$$

$$\begin{cases} EICO(y) = 0.0407y^{-2.2069} & \text{if } y < 0.153 \\ EICO(y) = 0.216y^{-1.3175} & \text{if } y > 0.153 \end{cases} \quad (6.4)$$

The mission profile, including the instantaneous fuel flow rate at every point along the simulated trajectory, can be now exported from ASTOS software resulting in:

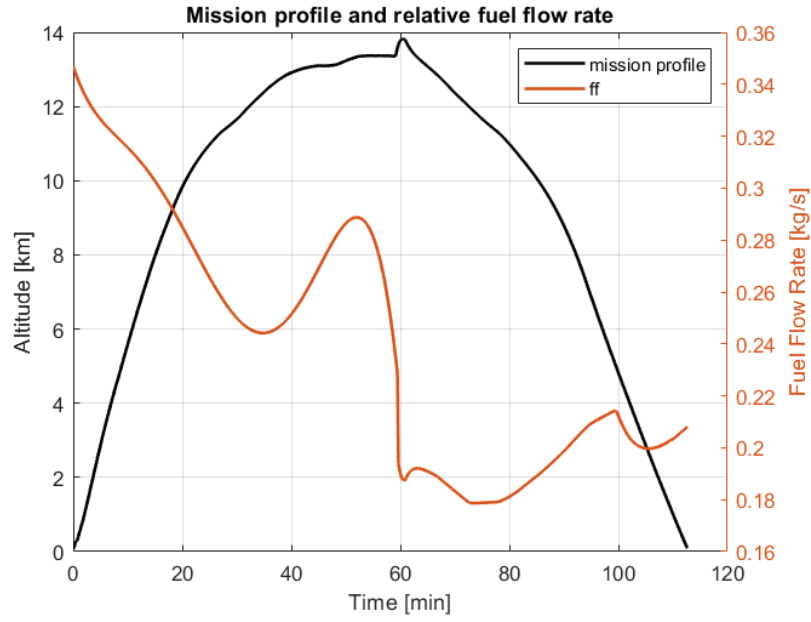


Figure 29: Reference mission trajectory and fuel flow

The fuel-flow curve in Figure 29 was interpolated in its initial portion, because the raw ASTOS output contained non-physical spikes, resulting from numerical integration errors. Applying the correction to adjust the fuel flow from flight level to sea level one obtains:

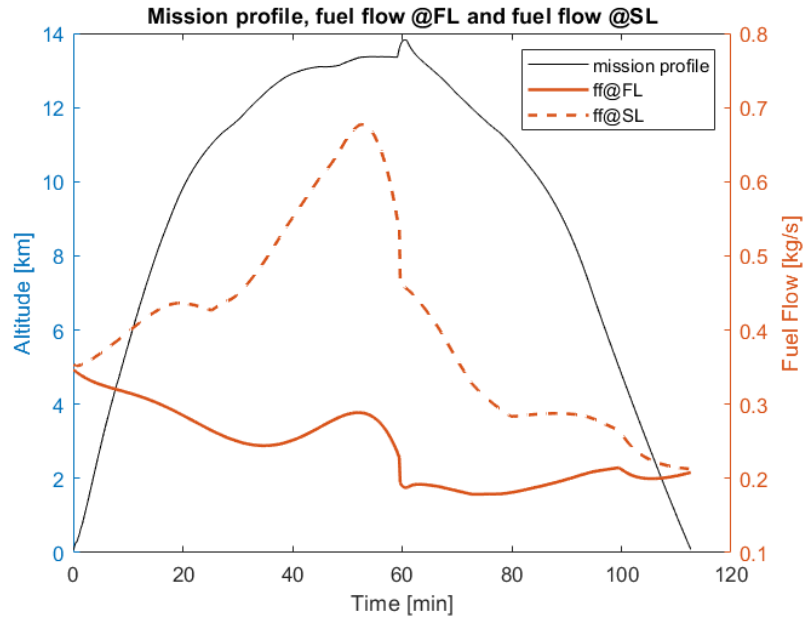


Figure 30: Correction of fuel flow from FL to SL

Entering the interpolation described by the equations 6.2,6.36.4 with the

fuel flow rate corrected at sea level for each mission point leads to:

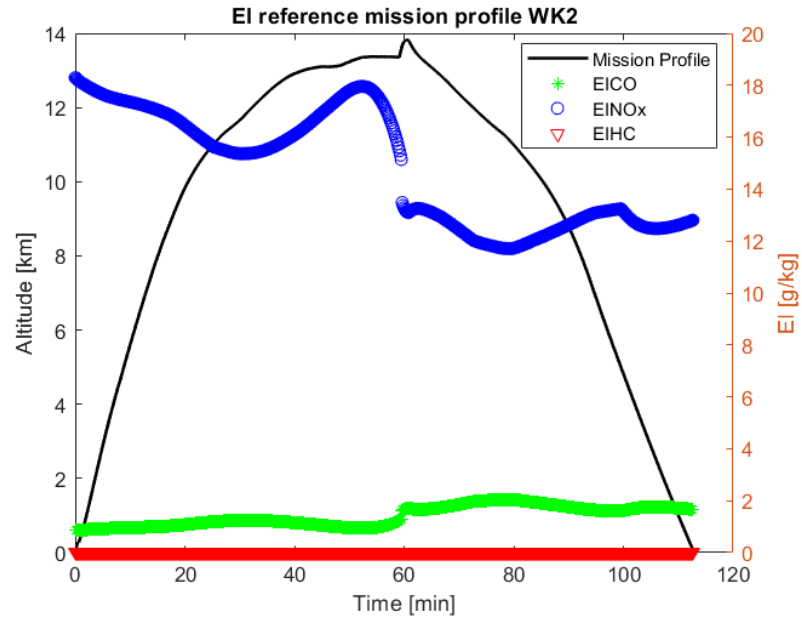


Figure 31: Emission indices through mission trajectory

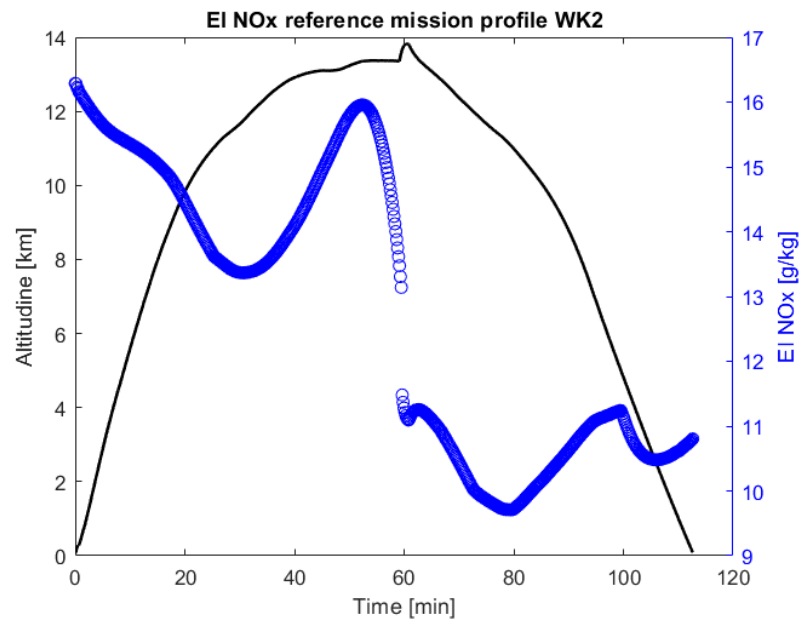


Figure 32: $EINO_x$ through mission trajectory

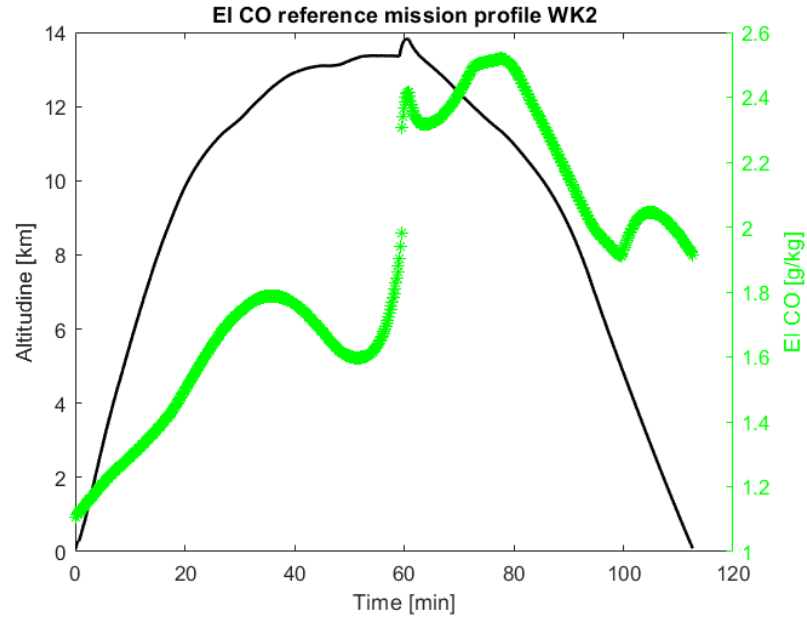


Figure 33: *EICO* through mission trajectory

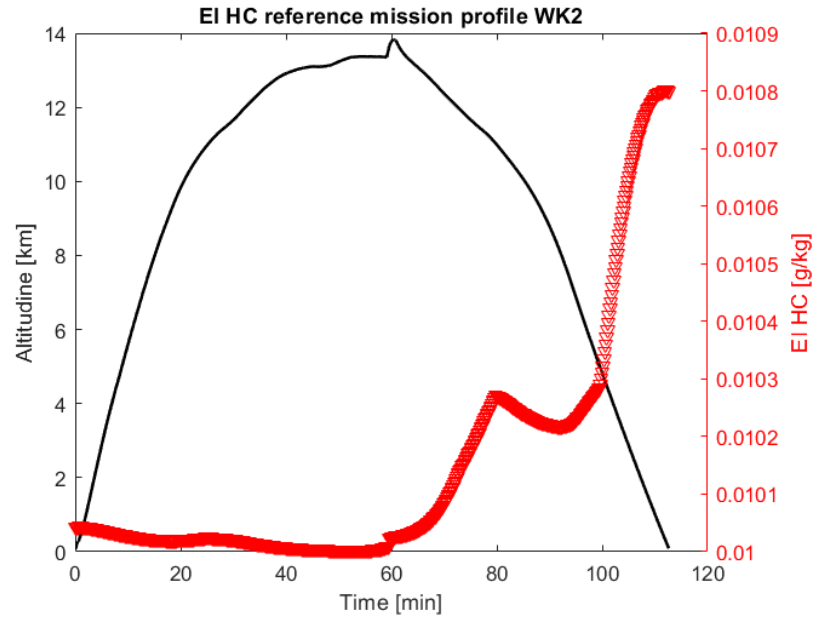


Figure 34: *EIHC* through mission trajectory

Finally, the total emissions for each pollutant considered can be calculated as follows:

$$M_{pollutant} = \sum_{i=1}^n EI_i * ff_i * dt_i \quad (6.5)$$

Where:

- EI = emission index of the considered pollutant for each instant of the mission;
- ff = fuel flow rate for each instant of the mission;
- dt = time between adjacent simulated point;
- n = number of simulated points that compose the mission trajectory.

Since ASTOS simulates the mission from liftoff to touchdown, it is necessary to simulate the takeoff and landing ground rolls and to include the contributions of these two segments, as well as the taxi-out and taxi-in phases, in the summation used to report the total mass of emitted chemical species calculated above.

As described in Chapter 5, these segments are modelled using Raymer's formulation.

For the take-off roll, from brake release to liftoff, the following inputs were fed into Eq. 5.2 to compute the instantaneous acceleration, which was then integrated to obtain velocity and distance travelled until $V < V_{TO}$:

- $W = 31840 + 13600$ kg (MTOW WK2 and SS2);
- $\mu = 0.03$ (from Figure 20);
- $T = 0.7 \cdot 123000$ kN;
- $\Lambda_{25} = 0$ (unswept wing);
- $C_{Lmax2D} = 2.6$ (assuming single slotted flap from 21);
- $\Delta C_{Lmaxflap} = 1.15$ (assuming single slotted flap from 21);
- $S = 200$ m²;
- $C_{Lmaxclean} = 1.45$ (from CFD simulation in mated configuration);
- $C_{D0} = 0.0367$ (from CFD simulation in mated configuration);
- $V_s = \sqrt{\frac{2W}{\rho S C_L}}$;
- $V_{TO} = 1.1 V_s$ (from Raymer's formulation);

The numerical integration leads to a comprehensive covered distance of 922 in 33.6 s, considering both ground-roll and rolling phase.

For the landing phase, from touchdown to full stop, the same input as above,

except for the ones following, were fed into Eq. 5.2 to compute the instantaneous acceleration, which was then integrated to obtain velocity and distance travelled until $V > 0$:

- $W = 31840 \cdot 0.85$ (as suggested from Raymer to take into account the fuel consumption);
- $\mu = 0.5$; (slightly different from takeoff condition because of the brakes);
- $T = 0.125 \cdot 123000 \text{ kN}$ (idle's power as Raymer suggests);
- $C_{L_{maxclean}} = 1.3$ (from CFD simulation in single configuration);
- $C_{D0} = 0.0301$ (from CFD simulation in single configuration);
- $V_{TD} = 1.15V_s$ (from Raymer's formulation);

The numerical integration yields a comprehensive covered distance of 542 meters in 19 seconds, considering both free-roll and braking distances.

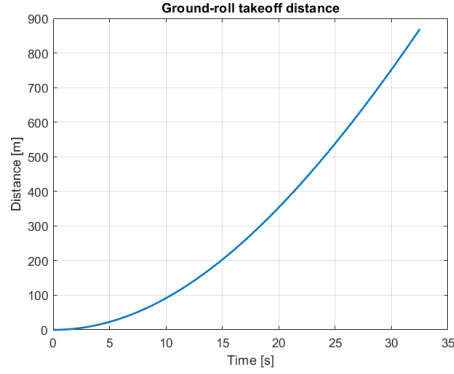


Figure 35: Ground-roll TO distance

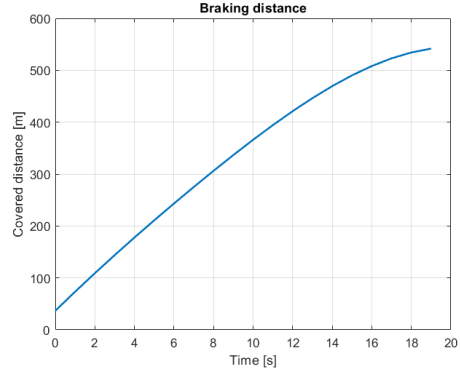


Figure 36: Braking distance

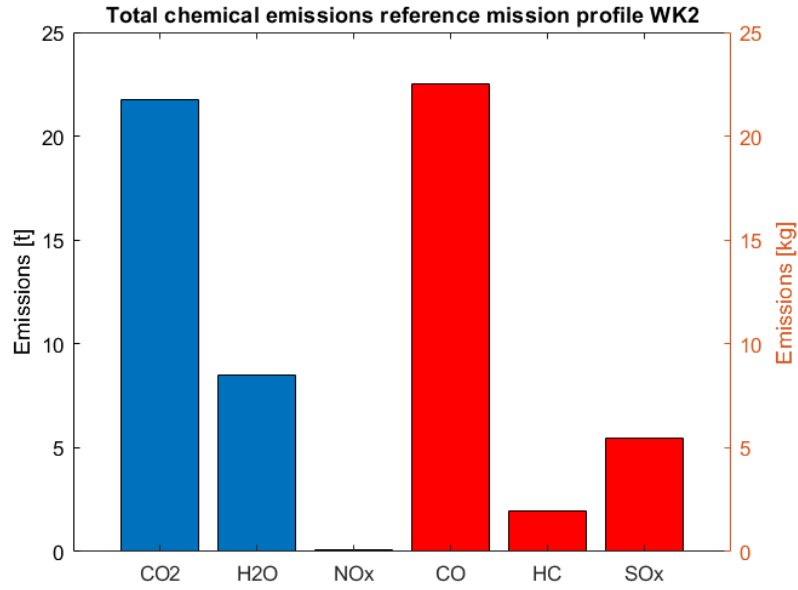


Figure 37: Total chemical emission WK2 reference trajectory

| Species | CO_2 | CO | H_2O | NO_x | SO_x | HC |
|-----------------------|--------|-------|--------|--------|--------|------|
| Emissions [kg] | 21746 | 22.54 | 8477 | 87.65 | 5.47 | 1.95 |
| Emissions [pounds] | 47950 | 49.70 | 18692 | 193.28 | 12.06 | 4.3 |
| Ref Emission [pounds] | 50579 | 26.44 | 20093 | 200.81 | 20.77 | - |

Table 12: Chemical emission WK2 reference trajectory

In Table 12 are reported the estimation of the total chemical emission of WK2 on its reference trajectory from and to Grottaglie spaceport. The last row, reports data from the FAA’s report [2], where Emissions from White Knight Two above 916 m were estimated by assuming a one-hour climb to the release altitude (15000 m) with engines at climb-out power, followed by a one-hour return flight after SpaceShipTwo’s release, during which engines operated at approach power.

The discrepancy between the results obtained using BFFM2 and those reported by the FAA arises from differences in the simulated mission: this work considers emissions from idle-to-idle, including those below 916 m, and models fuel-flow rate fluctuations during climb and approach based on ASTOS simulation data rather than assuming a constant rate.

Nevertheless, the results obtained by implementing BFFM2 are consistent and can be used to validate the model. Both proportional and non-proportional species show coherence:

- For proportional species, this confirms that the ASTOS-derived fuel-flow rates and discrete time intervals are reliable;
- For non-proportional species, it indicates that the method is correctly implemented and yields accurate results.

The only species lacking correspondence is SO_x . This discrepancy was also present in the LTO-cycle emission results, where fuel-flow rates and phase durations are prescribed by ICAO regulations, so the issue certainly lies with the emission index used (here 0.8 g/kg, from the literature [32]).

7 Air quality impact assessment results

This section will provide the results obtained implementing the methodology expressed in Chapter 5 about local air quality impact assessment.

7.1 NO_x average concentration in the engine plume - analytical model

The first part of the air quality assessment refers to implementing a simple analytical model to predict the average NO_x concentration in the engine plume during the takeoff phase.

Regarding the validation of the implementation of the Gaussian plume simplified formulation, it has been taken as a benchmark the average NO_x concentration of B373-3Q8, powered by the certified engine CFM56-3B2.

The pollutant mass rate has been calculated from the ICAO Emission database [12] as:

$$Q = EINO_x \cdot ff = 19.4 \cdot 1.056 = 20.49 \text{ g/s} \quad (7.1)$$

It was considered a constant emission of Q from a single static source for 1 minute (duration of takeoff phase) then it was averaged in time for each point of the grid, obtaining:

| | Aircraft | Engine | Calculated concentration | | Measured concentration | |
|----|-----------|------------|---------------------------------------|-------------|---------------------------------------|-------|
| | | | NOx (delta), $\mu\text{g}/\text{m}^3$ | | NOx (delta), $\mu\text{g}/\text{m}^3$ | |
| | | | with jet | without jet | value | error |
| 1 | B737-3YO | CFM56-3C1 | 27,43 | 30,01 | 31,8 | 3,2 |
| 2 | B737-3Q8 | CFM56-3B2 | 30,7 | 33,50 | 28,0 | 2,8 |
| 3 | B737-4SS | CFM56-3B2 | 29,76 | 27,95 | 23,6 | 2,4 |
| 4 | B737-4Q8 | CFM56-3B2 | 31,28 | 34,93 | 56,9 | 5,7 |
| 5 | A-310 | CF6-80C2A8 | 88,86 | 122,12 | 86,1 | 8,6 |
| 6 | A-319 | CFM56-5B5 | 29,85 | 32,27 | 26,9 | 2,7 |
| 7 | B747-230 | CF6-50E2 | 163,63 | 205,37 | 82,5 | 8,2 |
| 8 | A-321-211 | CFM56-5B-3 | 81,78 | 89,74 | 43,3 | 4,3 |
| 9 | A320-214 | CFM56-5B-4 | 49,99 | 52,29 | 16,4 | 1,6 |
| 10 | B737-33A | CFM56-3B1 | 25,5 | 27,95 | 11,5 | 1,1 |

Figure 38: Average takeoff NOx concentration from Synlyo and Zaporozhets's paper

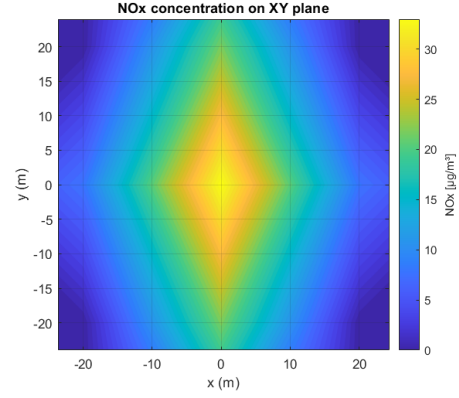


Figure 39: NOx average concentration during takeoff phase – B737-3Q8

The maximum averaged concentration is localized in proximity of the source and its value is $33.6 \mu\text{g}/\text{m}^3$, which is perfectly comparable with the results reported in the Kateryna Synlyo and Oleksandr Zaporozhets' paper [40], which describes the measured NOx concentrations in the aircraft engine plume (averaged over 1 minute) while the aircraft is accelerating on the runway during take-off stage and compares it with analytical data obtained by the application of PolEmiCa model.

Following the same procedure, it is possible to compute the maximum average concentration peak of NOx for White Knight Two and Boeing 747 LTO Dreamlifter. The data utilised are reported in Table 13.

| Aircraft | EINOx [g/kg] | Fuel flow [kg/s] | Duration [min] |
|-------------|--------------|------------------|----------------|
| WK2 | 16.74 | 0.36 | 1 |
| Dreamlifter | 34.36 | 2.725 | 1 |

Table 13: NOx dispersion analysis input data

The maximum average concentration of NOx is reported in Table 14:

| | WK2 | Dreamlifter |
|--------------------------------|------------------------------|---------------------------------|
| Max Averaged NOx concentration | $9.9 \mu\text{g}/\text{m}^3$ | $153.74 \mu\text{g}/\text{m}^3$ |

Table 14: Maximum Average NOx concentration - WK2 vs. Dreamlifter

Since the LTO cycle emissions of the Dreamlifter are higher than those of WK2, it is expected, and has been confirmed, that the NO_x concentration is also higher in the takeoff phase.

As asserted before, these data can be a valuable source to convince involved

people to accept suborbital flight operations from Grottaglie airport, since the local air quality and consequently their life quality would not be affected in a significant way.

7.2 Assessment of NO_x dispersion during WK2 LTO cycle operations using LASPORT

The second stage of the air quality impact assessment involves evaluating the concentration of NO_x during the phases of the ICAO LTO cycle at Taranto-Grottaglie Airport, carried out by the White Knight Two carrier.

7.2.1 Calculation setup

Regarding the calculation setup, as expressed in Chapter 5, 3 cases were simulated: departure, arrival, and idle.

Regarding the departure phase, it comprises takeoff and climb from runway 35 with 3 m/s headwind. The ground takeoff takes place from velocity zero to lift-off velocity over a distance of 922 m (accordingly to the ground-roll simulation performed using Raymer's equation and expressed in Chapter 6.2).

For the climb, a sequence of points (longitude, latitude, height, time, speed) were provided in an XLS coming from ASTOS simulation.

The takeoff and climb profiles created for LASPORT are:

[TABLE.PROFILES.INDIVIDUAL.DEPARTURE]

| Time(s); | Distance(m); | Altitude(m); | Velocity(m/s); | Mode |
|----------|--------------|--------------|----------------|------|
| 0.00; | 0.00; | 0.00; | 0.00; | TG |
| 33.60; | 922.00; | 0.00; | 89.44; | TG |
| 39.60; | 1471.84; | 34.49; | 94.06; | TG |
| 42.27; | 1724.64; | 54.00; | 95.79; | TG |
| 52.27; | 2562.01; | 140.53; | 92.23; | CI |
| 62.27; | 3500.26; | 212.44; | 95.41; | CI |
| 72.27; | 4238.81; | 209.92; | 93.49; | CI |
| 82.27; | 5187.69; | 281.81; | 96.85; | CI |
| 92.27; | 6164.99; | 362.11; | 99.42; | CI |
| 102.27; | 7164.87; | 447.49; | 101.47; | CI |
| 112.27; | 8183.04; | 536.79; | 103.18; | CI |
| 122.27; | 9217.03; | 629.32; | 104.69; | CI |
| 132.27; | 10233.85; | 694.37; | 106.77; | CI |
| 142.27; | 11302.41; | 793.69; | 107.79; | CI |
| 152.27; | 12380.39; | 894.57; | 108.68; | CI |

Figure 40: Departure profile

For what concerns the arrival, it is composed by the approach and the

landing ground roll phases to runway 35 with 3 m/s headwind.

Approach takes place with an angle of 3° to the horizontal (accordingly to ASTOS data). Distance from touchdown to roll-off was specified as 542 m with a final velocity of 0 m/s and a time of 19 s (see 6.2). In LASPORT, a constant deceleration is assumed from touchdown to roll-off, which yields a velocity at touchdown of 57.05 m/s.

Finally, as regards idle phase, it is considered at a fixed position for 13 minutes (half of the ICAO LTO cycle specification). In the LASPORT run, this position was located right before the start point of ground take-off.

In Table are reported the resulting times-in-mode (up to 895 m above ground level), the given NO_x emission rates (assuming 4 engines) and the resulting emissions per mode.

| Case | Departure | | Arrival | | Idle |
|---------------------|---------------------------|-------------------------|--------------------------|---------------------------|------------------------|
| LASPORT mode | TG ground/ take-off | CI climb/ initial | AF approach/ final | AG approach/ ground | ID idle/ taxiing |
| Time-in-mode (s) | 42.3 | 110.0 | 299.3 | 19.0 | 780.0 |
| Emission rate (g/s) | 24.12 | 21.80 | 11.00 | 3.42 | 0.656 |
| Emission (kg) | 1.020 | 2.398 | 3.292 | 0.065 | 0.512 |

Table 15: LASPORT setup data

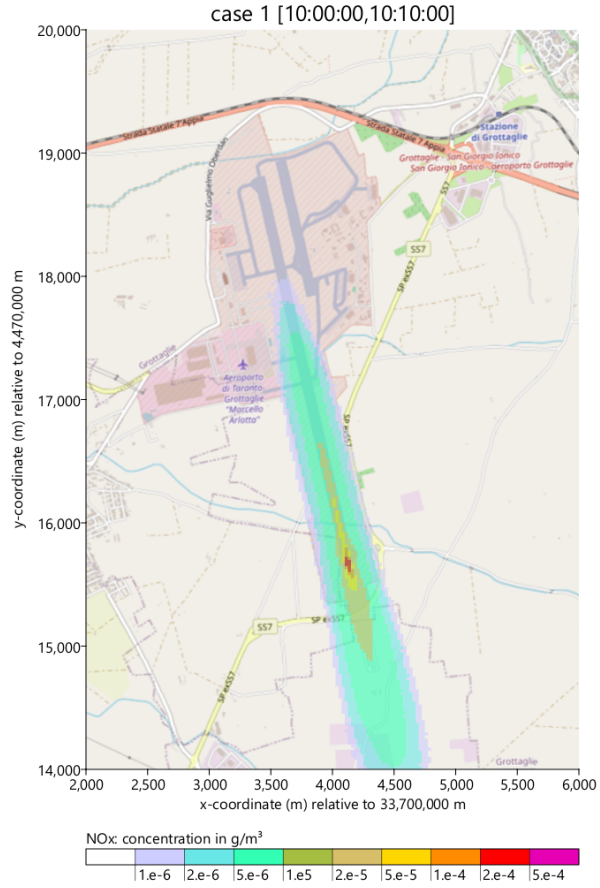
The three phases were prepared as three individual movements separated by about two hours.

7.2.2 Calculation results

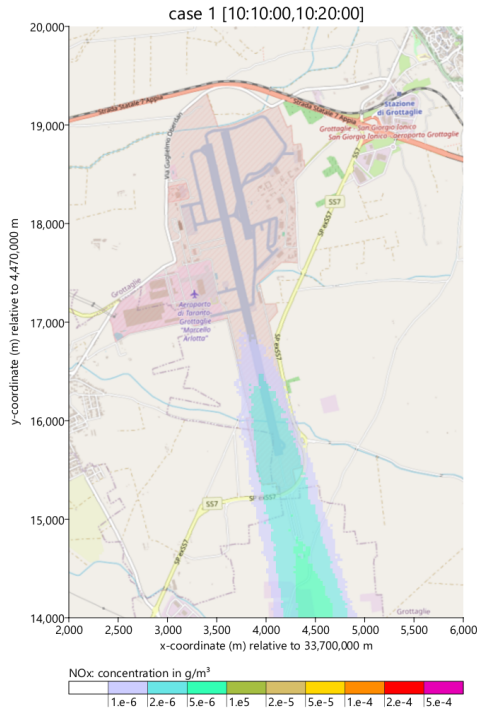
The near-ground concentration (averaged over the vertical interval from 0 m to 3 m above ground) was calculated with a horizontal resolution of 25 m and recorded as successive 10-minute averages. The movement times were selected to align the start of the first 10-minute interval with the beginning of the phase.

| Case | Specification |
|-----------|---|
| Departure | start of ground take-off (10:00:00) |
| Arrival | 10 minutes before roll-off at 12:00:00 (11:50:00) |
| Idle | start of idle (14:00:00) |

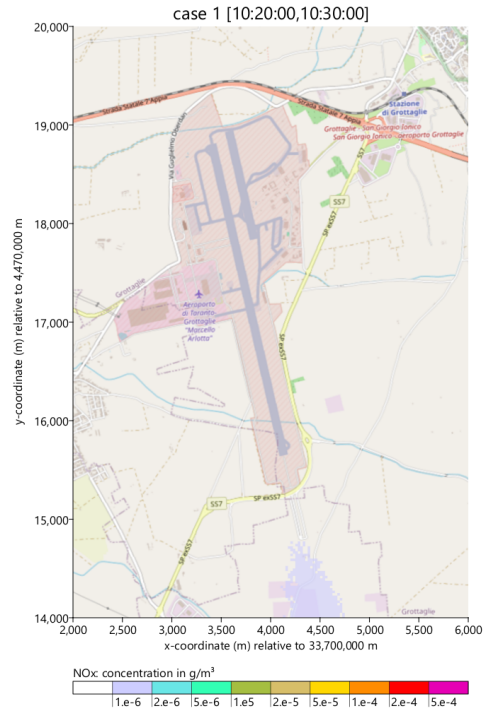
Table 16: Timing specifications for each case



(a) case 1 [10:20:00, 10:30:00]

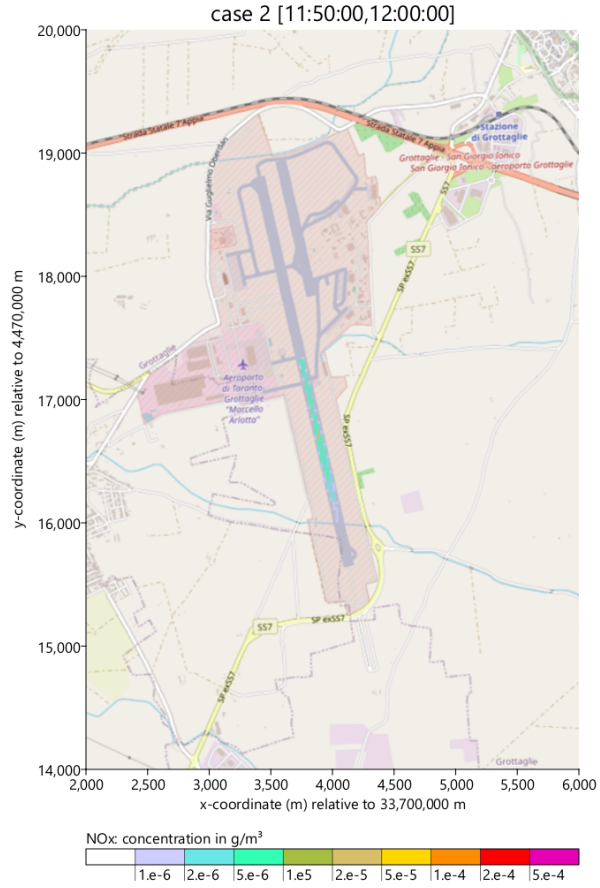


(b) case 1 [10:00:00, 10:10:00]

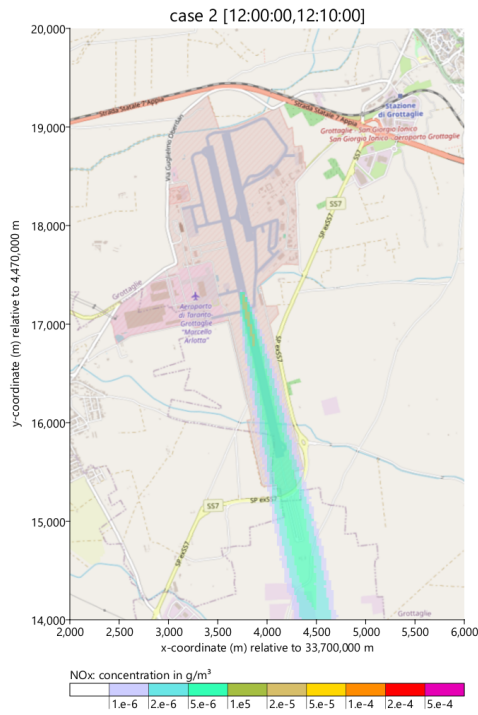


(c) case 1 [10:10:00, 10:20:00]

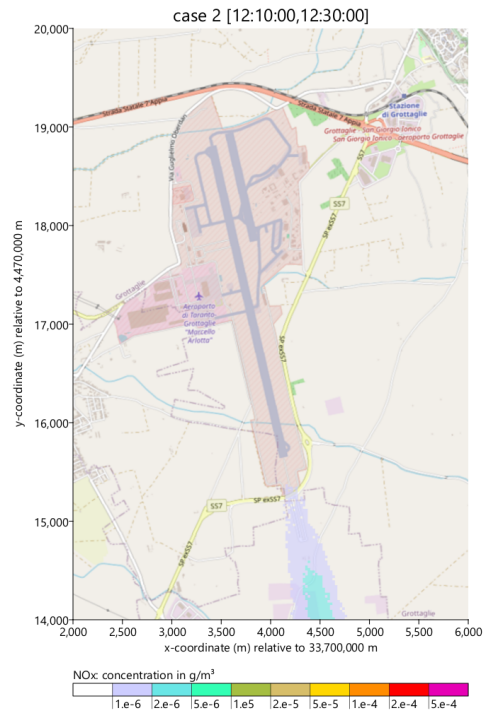
Figure 41: Case 1 (departure from runway 35, start ground take-off at 10:00:00): Successive 10-minute averages of the near-ground concentration of NO_x.



(a) case 2 [12:10:00, 12:20:00]

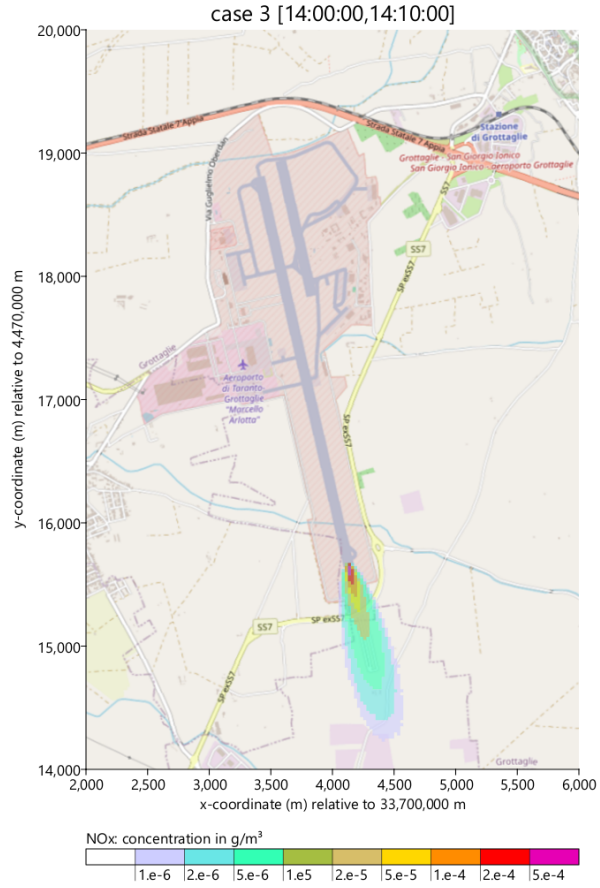


(b) case 2 [11:50:00, 12:00:00]

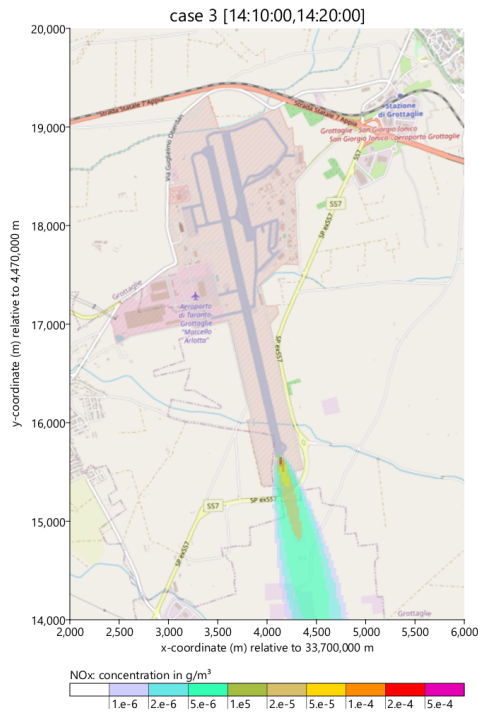


(c) case 2 [12:00:00, 12:10:00]

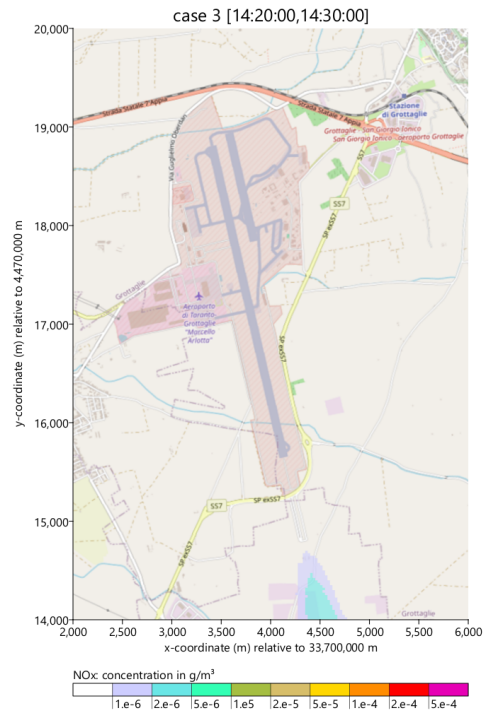
Figure 42: Case 2 (arrival at runway 35, roll-off at 12:00:00): Successive 10-minute averages of the near-ground concentration of NO_x.



(a) case 3 [14:00:00, 14:10:00]



(b) case 3 [14:10:00, 14:20:00]



(c) case 3 [14:20:00, 14:30:00]

Figure 43: Case 3 (idle at runway threshold at 14:00:00): Successive 10-minute averages of the near-ground concentration of NO_x.

The 10-minute concentration for the departure activity is of the order of:

$$C = \frac{16.74 \cdot 0.36 \cdot 60}{4000 \cdot 200 \cdot 200} = 10^{-5} \text{ g/m}^3 = 10 \text{ } \mu\text{g/m}^3 \quad (7.2)$$

which is in line with Figure 41a.

Regarding the approach operation, the first 10-minute interval shows only a small concentration because near-ground emissions occur only during the last minute of that period. In the second interval, using the same estimation method, the near-ground emitted mass is roughly 100 g (AG) plus 800 g (AF, including the downshift caused by wing-vortex interaction as accounted for in LASPORT), resulting in a concentration on the order of $10 \text{ } \mu\text{g/m}^3$, which aligns with the values reported in Figure 42b. The final 10-minute interval shows low concentrations in the southern area of runway 35.

Regarding the idle simulation, during the first 10 minutes (while emissions are still ongoing), a strong and concentrated NO_x plume is visible, with peak concentrations observed directly at the emission source and immediately downwind. In the following 10-minute interval, after emissions have ceased, dispersion reduces the visibility of the peak. The final 10 minutes of the simulation are characterized by very low concentrations, approximately 1 km from the emission source.

According to the EU Ambient Air Quality Directive 2008/50/EC, the annual mean concentration of NO_2 must not exceed $40 \text{ } \mu\text{g/m}^3$ and the hourly mean $200 \text{ } \mu\text{g/m}^3$ (no more than 18 exceedances per year) [11].

The concentrations of NO_x resulting from WK2 operations for each LTO phase are well below the regulatory limits. It should also be noted that the average is calculated over 10-minute intervals, with a total of three evaluations, always covering less than one hour. Therefore, while the hourly mean concentrations are clearly below the reported threshold values, it should be noted that European regulations take into account the total NO_x concentration from all airport-related traffic. Considering that, this assessment is not comprehensive.

8 Conclusion and future works

This work fits into the emerging scenario of European interest in suborbital flights, where unconventional flights are attracting increasing interest from both public and private companies. They are rapidly developing due to their flexibility, which makes them adaptable to various sectors and applications. Their versatility is evident: they are extremely valuable for scientific progress, as they enable experiments in microgravity conditions. In addition, they can be used for astronaut and pilot training, as well as for space tourism.

This thesis aimed to investigate the environmental impact of an A-to-A suborbital flight from and to Grottaglie airport, estimating the chemical emissions throughout the mission and evaluating the impact on local air quality.

The environmental impact of WK2 carrier operations enabling SS2's ascent to microgravity conditions has been found to be lower than expected, falling below that of currently operated flights at the studied airport (e.g., Boeing Dreamlifter scheduled flights). The data obtained implementing the BFFM2 has been demonstrated to be sufficiently accurate and were validated against documented data reported by FAA. This evaluation could serve as a starting point for a public acceptance campaign for nearby airport residents, promoting the transformation of this infrastructure into a spaceport capable of accommodating scheduled suborbital flights.

To expand the work, the analysis of the chemical emissions along the reference trajectory might be placed on a deeper level by designing the engine model capable of providing the necessary data to implement the $P_3 - T_3$ method, which is known to yield more accurate estimations.

Moreover, the mission simulation could be improved, taking into account the real on-ground path of the vehicles from gate to runway and back. This will be helpful for the evaluation of local air quality impact, too.

The assessment of the local air quality impact proved to be the most challenging aspect of this work. An extensive literature review led to the implementation of a simple analytical model to estimate the average concentration of NO_x during the takeoff phase, treating the source as continuous and static. This is undoubtedly just the first step in an analysis that can be further deepened and will be extremely valuable for the development of future regulations and technologies.

The computed concentration peak resulting from the takeoff operation of WK2 is lower than that produced during the same LTO cycle phase by the Boeing Dreamlifter, which operates weekly flights to and from the reference airport.

These findings are consistent with the comparison of LTO cycle emissions between WK2 and the Dreamlifter, which shows that the latter emits significantly more chemical species than the former.

Furthermore, a dispersion analysis of the departure, approach, and idle phases was carried out using the LASPORT tool. The simulations show the evolution of concentrations over 10-minute intervals for the carrier White Knight Two, using input data from the ASTOS simulated mission, Raymer's equations, and the Boeing Fuel Flow Method 2. These results can serve as a first step toward implementing broader simulations that include all airport-related traffic during a typical day at Taranto-Grottaglie Airport. They also provide a framework for evaluating the potential impacts of emerging aerospace operations, such as suborbital flights or commercial spaceports, which could become increasingly relevant in the coming years.

It would also be extremely interesting to evaluate the differences between tools based on different approaches to the dispersion problem. A comparison between the results obtained using the LASPORT tool (Lagrangian model) and, for example, CALPUFF (Gaussian puff model) could be important to identify the most suitable approach for the problem under examination.

To conclude, this study has adopted a highly simplified approach to evaluating the impact on air quality, intended as a first step into the vast field of pollutant dispersion analysis. However, this remains a complex issue to address, as it depends not only on aircraft operations but also on emissions from ground support equipment, auxiliary power units, and ground transportation to and from the airport. Consequently, future work could adopt a more holistic perspective by analysing pollutant concentrations over longer timeframes, such as monthly or yearly scales, while considering all relevant sources of emissions. Incorporating real meteorological data, variable traffic patterns, and validated chemical transformation models would further enhance the accuracy and relevance of the simulation outcomes.

References

- [1] Umweltmeteorologie – atmosphärische ausbreitungsmodelle – gaußsches fahnenmodell zur bestimmung von immissionskenngrößen, January 2016. Supersedes VDI 3782 Blatt 1:2009-08.
- [2] Federal Aviation Administration. Final environmental assessment for mojave spaceport and spaceshiptwo, 2012.
- [3] S. Pal Arya. *Air Pollution Meteorology and Dispersion*. Oxford University Press, 1999.
- [4] Steven L. Baughcum, Terrance G. Tritz, Stephen C. Henderson, and David C. Pickett. Scheduled civil aircraft emission inventories for 1992: Database development and analysis. appendix d: Boeing method 2 fuel flow methodology description. NASA Contractor Report 4700, National Aeronautics and Space Administration, Langley Research Center, April 1996. Appendix D.
- [5] National Transportation Safety Board. In-flight breakup during test flight, scaled composites spaceshiptwo, n339ss, near koehn dry lake, california, october 31, 2014. Aerospace Accident Report AAR-15/02, National Transportation Safety Board, Washington, DC, July 2015. PB2015-105454. Adopted July 28, 2015.
- [6] G. A. Briggs. Plume rise. Technical Report TID-25075, U.S. Atomic Energy Commission, Oak Ridge, Tennessee, 1969. Available from the Oak Ridge National Laboratory.
- [7] G. A. Davidson. A modified power law representation of the pasquill-gifford dispersion coefficients. *Journal of the Air & Waste Management Association*, 40(8):1146–1147, 1990.
- [8] dSPACE GmbH. Cooperating partners: Astos solutions. https://www.dspace.com/en/inc/home/company/cooperations/cooperating_partners/astos-solutions.cfm#179_80103, 2025.
- [9] D. DuBois and G. C. Paynter. Fuel flow method 2 for estimating aircraft emissions. Technical Paper 2006-01-1987, SAE International, Washington, DC, USA, 2006. SAE Technical Paper Series.

- [10] Ente Nazionale Aviazione Civile (ENAC). Regolamento per le operazioni suborbitali e di accesso allo spazio (saso), November 2023.
- [11] European Commission. Eu air quality standards. https://environment.ec.europa.eu/topics/air/air-quality/eu-air-quality-standards_en, 2024.
- [12] European Union Aviation Safety Agency (EASA). ICAO Aircraft Engine Emissions Databank. <https://www.easa.europa.eu/en/domains/environment/icao-aircraft-engine-emissions-databank>, n.d.
- [13] Federal Aviation Administration, Office of Commercial Space Transportation. Final Environmental Assessment and Finding of No Significant Impact for the Launch and Reentry of SpaceShipTwo Reusable Suborbital Rockets at the Mojave Air and Space Port. Environmental Assessment and Finding of No Significant Impact HQ-121575, Federal Aviation Administration, Office of Commercial Space Transportation, May 2012.
- [14] German Aerospace Center (DLR). Spaceliner rlv – hypersonic transport concept. Online Event Page, ILA Berlin Air Show 2018, 2018. Published: April 2018.
- [15] A. E. S. Green, R. P. Singhal, and R. Venkateswar. Analytic extensions of the gaussian plume model. *Journal of the Air Pollution Control Association*, 30(7):773–776, 1980.
- [16] Aritra Guha. NO_x prediction using combustion emissions modeling. *AIAA Journal of Propulsion and Power*, 28(3):624–632, 2012.
- [17] Ingenieurbüro Janicke. *AUSTAL2000: German Federal Environmental Agency Dispersion Model*. Umweltbundesamt (German Federal Environmental Agency), Langen, Germany, 2003. Version 1.1, English Translation.
- [18] International Atomic Energy Agency (IAEA). Introduction to atmospheric dispersion process and models. Webinar Presentation, 7th MEREIA Webinar on Basic Concepts, March 2023. PDF downloaded from IAEA GNSSN.
- [19] International Civil Aviation Organization (ICAO). *Airport Air Quality Manual, Third Edition*. International Civil Aviation Organiza-

- tion, 3 edition, 2023. Available online: <https://store.icao.int/en/airport-airquality-manual-doc-9889> (accessed on 1 November 2024).
- [20] International Civil Aviation Organization (ICAO). Local Air Quality — Environmental Protection. <https://www.icao.int/environmental-protection/pages/local-air-quality.aspx>, 2025. Consultado el 17 de junio de 2025.
- [21] U. Janicke. Application of Effective Conversion Rates between NO and NO₂ in a Standard Airport Dispersion Model System. *Atmosphere*, 15(574):431–447, 2024.
- [22] U. Janicke, E. Fleuti, and I. Fuller. LASPORT – A model system for airport-related source systems based on a Lagrangian particle model. In *Proceedings of the 11th International Conference on Harmonization within Atmospheric Dispersion Modeling for Regulatory Purposes*, Cambridge, Great Britain, 2007. Available online: https://www.harmo.org/Conferences/Proceedings/_Cambridge/publishedSections/Op352-356.pdf (accessed on 10 April 2025).
- [23] U. Janicke, E. Fleuti, and I. Fuller. LASPORT – a model system for airport-related source systems based on a Lagrangian particle model. In *Proceedings of the 11th International Conference on Harmonization within Atmospheric Dispersion Modeling for Regulatory Purposes*, Cambridge, Great Britain, 2007. Available online: https://www.harmo.org/Conferences/Proceedings/_Cambridge/publishedSections/Op352-356.pdf (accessed on 10 April 2025).
- [24] U. Janicke, E. Montreuil, W. Ghedhaïfi, and E. Terrenoire. Time resolved aircraft dispersion modelling. In *3rd ECATS Conference*, 2020.
- [25] Janicke Consulting. LASPORT: a program system for the calculation of airport-related pollutant emissions and concentrations in the lower atmosphere. Technical Report Version 2.3, Janicke Consulting, Überlingen, Germany, December 2018. Disponibile dal sito di Janicke Consulting.
- [26] Lakes Environmental Software. Austal2000: Program documentation (english). https://www.weblakes.com/products/austal/resources/docs/austal2000_en.pdf, February 2009. Program documentation for

version 2.4 of AUSTAL2000, a dispersion model implementing Appendix 3 of the German Regulation on Air Quality Control (TALuft).

- [27] Lakes Environmental Software. Calpuff modeling system. Online, 2024. Accessed: 2025-07-05.
- [28] Lakes Environmental Software. Calpuff view – puff air dispersion model. Online, 2025.
- [29] Christian Langner and Otto Klemm. A comparison of model performance between AERMOD and AUSTAL2000. *Journal of the Air & Waste Management Association*, 61(6):640–646, 2011.
- [30] H. Lorentz, U. Janicke, H. Jakobs, W. Schmidt, P. Hellebrandt, M. Ketzel, and H. Gerwig. Ultrafine particle dispersion modelling in the vicinity of the major airport Frankfurt/Main, Germany. In *Proceedings of the 19th International Conference on Harmonization within Atmospheric Dispersion Modeling for Regulatory Purposes*, Bruges, Belgium, 2019.
- [31] John Mettrop. 2019 world radiocommunication conference agenda item 1.6: Sub-orbital vehicles. https://www.icao.int/MID/Documents/2023/WRC-23%20and%20FSMP-SG17/FSMP-WG17-WRC23WrkShp21_WRC%20AI%201.6.pdf, 2023.
- [32] Axel Molander. Sustainable aviation fuels, the fuel of the future? a scenario analysis of saf using high resolution emission data. M.sc. thesis, KTH Royal Institute of Technology, Stockholm, Sweden, June 2024. Second cycle, 30 credit; approved 2024-06-17; Examiner: Frauke Urban; Supervisor: Emily Christley.
- [33] National Transportation Safety Board. In-flight breakup during test flight, scaled composites spaceshiptwo, n339ss, near koehn dry lake, california, october 31, 2014. Aviation Accident Report NTSB/AAR-15/02, National Transportation Safety Board, Washington, D.C., 2015.
- [34] Intergovernmental Panel on Climate Change (IPCC). *Aviation and the Global Atmosphere*. Cambridge University Press, Cambridge, UK, 1999. Table 7-2: Typical emission index (g/kg) levels for engine operating regimes.
- [35] International Civil Aviation Organization. Annex 16 to the convention on international civil aviation: Environmental protection. volume ii—aircraft

- engine emissions. International Standards and Recommended Practices AN16-2, International Civil Aviation Organization, Montréal, Québec, July 2017. Supersedes all previous editions on 1 January 2018.
- [36] Daniel P. Raymer. *Aircraft Design: A Conceptual Approach*. American Institute of Aeronautics and Astronautics, Reston, VA, sixth edition, 2018.
 - [37] H. Scholz. Aircraft Design – chapter 5: Preliminary sizing. Lecture notes, Hamburg University of Applied Sciences, n.d.
 - [38] L. L. Schulman and J. S. Scire. Development of the industrial source complex (isc) dispersion model. Technical Report EPA-600/4-80-029, U.S. Environmental Protection Agency, Research Triangle Park, NC, 1980. Prepared for the U.S. EPA Office of Research and Development.
 - [39] Joseph S. Scire, Dennis G. Strimaitis, and Robert J. Yamartino. *A User’s Guide for the CALPUFF Dispersion Model (Version 5)*. Earth Tech, Inc., Concord, MA, 2000. Downloaded from the official CALPUFF website.
 - [40] Kateryna Synylo and Oleksandr Zaporozhets. Polemica model for local air quality assessment in airports. In *16th Annual CMAS Conference*, page –, Chapel Hill, NC, USA, October 2017. Presented October 23–25, 2017.
 - [41] D. B. Turner. *Workbook of Atmospheric Dispersion Estimates*. U.S. Environmental Protection Agency, Office of Air Programs, 1970. Publication No. AP-26.
 - [42] U.S. Environmental Protection Agency. Air quality dispersion modeling – preferred and recommended models. Online, July 2021.
 - [43] U.S. Environmental Protection Agency. User’s guide for the ams/epa regulatory model (aermod). Technical Report EPA-454/B-24-007, U.S. Environmental Protection Agency, November 2024.
 - [44] VDI – The Association of German Engineers. Vdi 3783 part 8. environmental meteorology; turbulence parameters for dispersion models supported by measurement data. <https://www.vdi.de/en/home/vdistandards>, April 2017.
 - [45] Virgin Galactic. WK2 Data Brochure. Brochure, Virgin Galactic, oct 2020.

- [46] Wind Energy Group, Massachusetts Institute of Technology. Profile of relative humidity in the tropical atmosphere. <https://www.wind.mit.edu>, n.d.
- [47] World Meteorological Organization. *Guide to Meteorological Instruments and Methods of Observation*. WMO-No. 8. World Meteorological Organization, Geneva, Switzerland, 7th edition, 2008. Chapter I.5, page I.5-13.
- [48] Junli Yang, Likun Li, Xiaoyu Zheng, Hang Liu, Fengming Li, and Yi Xiao. Pollutant dispersion of aircraft exhaust gas during the landing and takeoff cycle with improved gaussian diffusion model. *Atmosphere*, 15(10):1256, 2024.